REPORT NO.
UCB/SEMM-89/13

STRUCTURAL ENGINEERING, MECHANICS AND MATERIALS

RESULTANT FIELDS FOR MIXED PLATE BENDING ELEMENTS

by

SHMUEL L. WEISSMAN

and

ROBERT L. TAYLOR

MAY 1989

**DEPARTMENT OF CIVIL ENGINEERING
UNIVERSITY OF CALIFORNIA
BERKELEY, CALIFORNIA**

Resultant Fields for Mixed Plate Bending Elements

Shmuel L. Weissman & Robert L. Taylor

Department of Civil Engineering
University of California, Berkeley

ABSTRACT

In this work the Hellinger-Reissner variational principle is used to formulate plate bending elements based upon Reissner-Mindlin plate theory. The formulation introduces an explicit coupling between interpolations of the shear and moment stress resultant fields. Because of the coupling, shear locking is avoided at the element level rather than at the global level. The coupling term is obtained by constraining the shear and moment resultant fields, that are initially assumed independent, to perform no work when subjected to a set of incompatible displacement modes. The resultant fields are formulated as a complete polynomial expansion in the element's natural coordinates and then transformed to the physical domain. Thus, frame invariant elements are always obtained. The resulting elements are shown to perform well on a set of standard problems for thin and thick plates.

1. Introduction

1.1 Background.

Plate bending solutions pose a difficult problem for the classical finite element displacement method. If the Kirchoff-Love plate theory is used, C^1 shape functions are required and the elements are restricted to thin plate applications. For this reason, most elements presented recently in the literature are based on a Reissner-Mindlin plate theory that requires only C^0 shape functions and also is applicable to both thin and thick plate applications. Unfortunately, many of the proposed elements fail at the thin plate limit because of a phenomenon known as shear locking.

Development of a general class of elements free of shear locking in all applications has been the focus of much research during the past two decades. The first successful developments were based upon reduced integration and selective reduced integration, concepts which were proposed simultaneously by Zienkiewicz, Taylor & Too [1971] and Pawsey & Clough [1971]. Malkus & Hughes [1978] demonstrated that both reduced integration and selective reduced integration fall within the scope of a mixed finite element method.

Unfortunately, reduced integration often leads to an unstable element because spurious zero-

energy modes are present. Selective reduced integration uses full integration on the bending term and reduced integration on the shear terms. Furthermore, selective reduced integration elements are rank deficient, and thus exhibit spurious zero-energy modes. By careful choice of the boundary conditions, however, these modes can be controlled (see e.g. Hughes [1987], pp. 334).

Hughes & Tezduyar [1981] presented a four-node element, known as T1, which is free of zero-energy modes. In addition, it does not exhibit shear locking on reasonable meshes. The T1 element was obtained by observing that the number of constraints on the element as a result of shear may be reduced by sharing terms across element boundaries. Thus, a non-locking element is obtained. A closely related formulation based upon the Hu-Washizu functional and discrete constraints on shear strains was presented by Bathe & Dvorkin [1984]. In the case of parallelogram elements, both formulations are identical.

Pian & Sumihara [1984] presented a plane stress element based upon the Hellinger-Reissner variational principle. The assumed independent stress field was subjected to constraint equations. These equations are interpreted as satisfying the equilibrium equations in a weak sense relative to assumed incompatible modes. Initially the formulation required a quadratic perturbation of the element shape in order to obtain the required number of independent constraint equations. Recently, Pian & Wu [1988] presented a new formulation which avoids element perturbation. The constraint equations are obtained by constraining the stress field to perform no work along the element boundary when subjected to a set of incompatible displacement modes.

1.2 Overview of the paper.

The objective of this paper is to present a formulation for plate elements based upon the Reissner-Mindlin plate theory, which is free from shear locking and spurious zero-energy modes.

The Hellinger-Reissner functional for plate bending is stated in terms of moment and shear resultant fields together with compatible and incompatible displacement fields. The terms associated with the incompatible modes are then required to vanish. This introduces constraints on the assumed independent shear and moment resultant fields. These constraint equations are used to reduce the number of independent coefficients in the shear and moment resultant fields. The final structure is

similar to the shear field presented by Bathe & Devorkin [1984] and a bending field similar to the Pian & Sumihara [1984] formulation. In addition, a coupling between the shear and moment stress resultant fields is introduced.

The independent resultant fields are assumed to be complete polynomials in the natural coordinates. The resultant fields are then transformed into physical coordinates. The coordinate transformation is similar to the one used to transform second Piola-Kirchhoff stresses into Cauchy stresses. In order to meet the patch test requirements, the coordinate transformation is based on only a constant value computed at the element center (Pian & Sumihara [1984]). It follows that the resulting elements are frame invariant.

Inclusion of the coupling terms results in elements that are free of shear locking. This will be proved and illustrated through the analysis of standard test problems. Imposing the coupling explicitly is consistent with the equilibrium equations and avoids introducing ad-hoc assumptions that would be necessary to overcome shear locking.

The proposed formulation is presented in Section 2. In Section 3, a proof is given in which, as thickness is reduced to zero, results obtained by the proposed elements converge to the thin plate solution and do not lock in shear. Section 4 presents the finite element approximations used for the four-node elements presented here. Numerical examples are presented in Section 5.

2. General formulation

Working within the framework of Reissner-Mindlin plate theory, the Hellinger-Reissner functional is used as the starting point for the new formulation. The first part of this section is devoted to the formulation of appropriate constraint equations. Application of the constraint equations to the stress resultant field approximations yields an explicit coupling between the assumed independent shear and moment resultant fields. In the second part of this section, the stiffness matrix is formulated.

Ignoring boundary terms, (which play no role in issues relating to shear locking), the Hellinger-Reissner functional can be stated as follows in the case of plate bending:

$$\Pi_R = \int_\Omega \left\{ -\frac{1}{2}(\mathbf{M}^T \mathbf{C} \mathbf{M} + \mathbf{Q}^T \mathbf{c} \mathbf{Q}) + \mathbf{M}^T \mathbf{L}^b \mathbf{U} + \mathbf{Q}^T \mathbf{L}^s \mathbf{U} \right\} d\Omega - \int_\Omega \mathbf{U}^T \mathbf{p}\, d\Omega \qquad (2.1)$$

where :

$\mathbf{C}$ - elastic compliances (bending).

$\mathbf{c}$ - elastic compliances (shear).

$\mathbf{L}^b$ - strain displacement operator (bending), given by:

$$\mathbf{L}^b = \begin{bmatrix} 0 & 0 & -\frac{\partial}{\partial x} \\ 0 & \frac{\partial}{\partial y} & 0 \\ 0 & \frac{\partial}{\partial x} & -\frac{\partial}{\partial y} \end{bmatrix}$$

$\mathbf{L}^s$ - strain displacement operator (shear), given by:

$$\mathbf{L}^s = \begin{bmatrix} \frac{\partial}{\partial x} & 0 & 1 \\ \frac{\partial}{\partial y} & -1 & 0 \end{bmatrix}$$

$\mathbf{U}$ - displacement field, given by: $\mathbf{U}^T = < w\ , \theta_x\ , \theta_y >$

$\mathbf{M}$ - moment resultant field, given by: $\mathbf{M}^T = < M_{xx}\ , M_{yy}\ , M_{xy} >$

$\mathbf{Q}$ - shear resultant field, given by: $\mathbf{Q}^T = < Q_x\ , Q_y >$

$\mathbf{p}$ - transverse body force.

Ω - domain of interest.

Γ_t - the part of the boundary of $\overline{\Omega}$ (closure of Ω) on which tractions are specified.

Sign conventions for the rotations are shown in figure 2.1, and sign conventions for shear and moment resultants are shown in figure 2.2.

The first variation of (2.1) yields:

$$\delta\Pi_R = \int_\Omega \delta\mathbf{M}^T (\mathbf{L}^b \mathbf{U} - \mathbf{C}\mathbf{M})\, d\Omega + \int_\Omega \delta\mathbf{Q}^T (\mathbf{L}^s \mathbf{U} - \mathbf{c}\mathbf{Q})\, d\Omega$$
$$+ \int_\Omega \left\{ (\mathbf{L}^b \delta\mathbf{U})^T \mathbf{M} + (\mathbf{L}^s \delta\mathbf{U})^T \mathbf{Q} - \delta\mathbf{U}^T \mathbf{p} \right\} d\Omega$$

The first two terms are the constitutive equations. After integration by parts, the last term in combi-

nation with the traction boundary conditions, provides balance of momentum equations for the plate.

A finite element solution based upon (2.1) requires the approximation of M and Q in Ω and U in $\Omega \bigcup \Gamma_t$. In this study, the stress resultants M and Q are approximated independently in each element. The displacement parameters are approximated by the sum of compatible and incompatible displacement fields. The incompatible fields satisfy constraints to ensure that the patch test is satisfied (Taylor, Zienkiewicz, Simo & Chan [1986]). Accordingly, the displacement field approximation is written as:

$$\mathbf{U} = \mathbf{U}^c + \mathbf{U}^i$$

where :

$\mathbf{U}^c$ - compatible displacement field.

$\mathbf{U}^i$ - incompatible displacement field.

(2.1) may now be written as:

$$\Pi_R = \int_\Omega \left\{ -\frac{1}{2}(\mathbf{M}^T \mathbf{C} \mathbf{M} + \mathbf{Q}^T \mathbf{c} \mathbf{Q}) + \mathbf{M}^T \mathbf{L}^b (\mathbf{U}^c + \mathbf{U}^i) + \mathbf{Q}^T \mathbf{L}^s (\mathbf{U}^c + \mathbf{U}^i) \right\} d\Omega - \int_\Omega \mathbf{U}^c \, \mathbf{p} \, d\Omega \qquad (2.2)$$

In (2.2), it is assumed that the work done by the loading term on the incompatible displacements may be ignored so that variation with respect to the incompatible displacements yields the following :

$$\delta\Pi_i = \int_\Omega (\mathbf{M}^T \mathbf{L}^b \, \delta\mathbf{U}^i + \mathbf{Q}^T \mathbf{L}^s \, \delta\mathbf{U}^i) \, d\Omega = 0 \qquad (2.3)$$

Satisfaction of (2.3) leads to a set of constraints on the stress resultant fields approximation. These constraints can be used to reduce the number of independent parameters in M and Q. If M and Q satisfy (2.3), then, because of the bilinear structure of (2.3), all references to the incompatible displacements disappear since:

$$\Pi_i = \int_\Omega \left\{ \mathbf{M}^T \mathbf{L}^b \mathbf{U}^i + \mathbf{Q}^T \mathbf{L}^s \mathbf{U}^i \right\} d\Omega = 0$$

Furthermore, this condition is met if the overall solution is required to be independent of incompatible modes and thus, to satisfy general uniqueness conditions.

In this study, each element is used as the domain in which these constraints are satisfied. The moment resultants M and shear resultants Q are approximated by a polynomial expansion in each

element. Incompatible modes are introduced to ensure that the resulting elements are free from spurious zero-energy modes and to prevent shear locking in the thin plate limit. The latter point is proved in Section 3 and a set of numerical examples is used to demonstrate the technique in Section 5.

2.1 Constraint equations.

Because incompatible displacements are present in (2.2), internal energy is dependent upon the internal partition of the domain. It follows that the internal energy may not be uniquely defined nor may it necessarily equal the external energy. In order to overcome this problem, the energy produced by the incompatible displacements is constrained to be zero. As shown above, this is equivalent to setting the variation with respect to $\mathbf{U}^i$ equal to zero. The following constraint is introduced :

$$\Pi_i = \int_\Omega \left\{ \mathbf{M}^T \mathbf{L}^b \mathbf{U}^i + \mathbf{Q}^T \mathbf{L}^s \mathbf{U}^i \right\} d\Omega = 0 \tag{2.4}$$

Evaluation of (2.4) using the definitions for $\mathbf{L}^b$ and $\mathbf{L}^s$ yields the set of independent equations:

$$\begin{aligned} \Pi_{i1} &= \int_\Omega \left\{ q_x \; w^i_{,x} + q_y \; w^i_{,y} \right\} d\Omega = 0 \\ \Pi_{i2} &= \int_\Omega \left\{ M_{yy} \theta^i_{x,y} + M_{xy} \theta^i_{x,x} - q_y \theta^i_x \right\} d\Omega = 0 \\ \Pi_{i3} &= \int_\Omega \left\{ M_{xx} \theta^i_{y,x} + M_{xy} \theta^i_{y,y} - q_x \theta^i_y \right\} d\Omega = 0 \end{aligned} \tag{2.5}$$

Since moment and shear resultants are approximated independently in each element, these constraints may be imposed on each individual element.

It should be noted that the above equations are independent of material properties and are therefore generally applicable. In finite element application, the above equations provide a set of algebraic equations on each element, which may be used to reduce the number of independent parameters in the stress resultant fields approximation. The number of constraint equations for each element is defined by the number of independent terms in the incompatible displacement field $\mathbf{U}^i$.

In addition to the above constraints, $\mathbf{U}^i$ is selected so that elements pass the patch test. Accordingly, for a constant stress resultant state, the approximation for $\mathbf{U}^i$ is required to satisfy:

$$\int_{\Omega} w^i_{,\alpha}\, d\Omega = 0$$

and

$$\int_{\Omega} \theta^i_{\alpha,\beta} d\Omega = 0$$

where both α and β may stand for x or y.

It should be noted that θ_α is not constrained since this condition does not result from a constant overall stress resultant state (i.e., these constants, Q_α, would require $M_{\alpha,\beta}$ to vary linearly in each element).

REMARK 2.1.1 : Equations (2.5) represent in each element 3n equations where n is the number of independent incompatible modes assumed in each element. Thus, the number of incompatible modes assumed can be deduced from the number of independent resultant parameters to be eliminated. Furthermore, the number to be eliminated may be assessed based on the required rank of the final stiffness matrix.

REMARK 2.1.2 : The structure of the constraint equations results in an explicit coupling between the shear and moment resultant fields, through $(2.5)_2$ and $(2.5)_3$. Although this coupling requires additional computation, it eliminates shear locking without resorting to ad-hoc assumptions. This coupling also is present in the equilibrium equations; thus, the constraint equations impose explicitly a consistent constraint form.

2.2 Stiffness matrix formulation.

Starting with the first variation of the Hellinger-Reissner functional, the Euler-Lagrange equations are deduced. Elimination of the stress resultants yields the stiffness matrix. In the remainder of this section, only the compatible displacement field is considered, since (2.5) is assumed to be satisfied. For simplicity the superscript c denoting compatible field is omitted.

At this point, it is essential to decide how the coupled system should be constructed. The structure of the constraint equations suggests the following choice† :

† Alternatives could couple the moment and/or shear interpolations.

$$\overline{\mathbf{M}} = \tilde{\mathbf{M}} m + \tilde{\mathbf{S}} q \tag{2.6a}$$

$$\overline{\mathbf{Q}} = \tilde{\mathbf{Q}} q \tag{2.6b}$$

where $\overline{\mathbf{M}}$ and $\overline{\mathbf{Q}}$ are the reduced resultant fields (i.e., those which satisfy (2.5)). The finite element approximation of the displacement field is :

$$\mathbf{U} = N_I \mathbf{d}_I$$

Where N_I is the (compatible) shape function associated with node I, summation convention is implied and $\mathbf{d}_I$ are the nodal displacements. Applying the strain displacement operators $\mathbf{L}^b$ and $\mathbf{L}^s$ to the assumed displacement field yields :

$$\mathbf{L}^b \mathbf{U} = \mathbf{B}_I^b \mathbf{d}_I$$

and

$$\mathbf{L}^s \mathbf{U} = \mathbf{B}_I^s \mathbf{d}_I$$

Where $\mathbf{B}_I^b$ and $\mathbf{B}_I^s$ are the finite element strain displacement matrices.

Utilizing the assumed fields as given above, the first variation of the Hellinger-Reissner functional is given by :

$$\begin{aligned} \delta\Pi_R = \int_\Omega [\, & \delta \mathbf{m}^T \, (-\mathbf{H}_{mm}^b \mathbf{m} - \mathbf{H}_{ms}^b \mathbf{q} + \mathbf{G}_m^b \mathbf{d} \,) + \\ & \delta q^T \, (-\mathbf{H}_{ms}^{bT} \mathbf{m} - \mathbf{H}_{ss}^b \mathbf{q} - \mathbf{H}^s \mathbf{q} + \mathbf{G}_s^b \mathbf{d} + \mathbf{G}^s \mathbf{d} \,) + \\ & \delta \mathbf{d}^T \, (\mathbf{G}_m^{bT} \mathbf{m} + \mathbf{G}_s^{bT} \mathbf{q} + \mathbf{G}^{sT} \mathbf{q} \,)] \, d\Omega = \delta \mathbf{d}^T \mathbf{f} \end{aligned} \tag{2.7}$$

where $\mathbf{f}$ is the force vector resulting from transverse loading and boundary conditions and

$$\begin{gathered} \mathbf{H}_{mm}^b = \int_\Omega \tilde{\mathbf{M}}^T \mathbf{C} \tilde{\mathbf{M}} \, d\Omega \;\; ; \;\; \mathbf{H}_{ms}^b = \int_\Omega \tilde{\mathbf{M}}^T \mathbf{C} \tilde{\mathbf{S}} \, d\Omega \;\; ; \\ \mathbf{H}_{ss}^b = \int_\Omega \tilde{\mathbf{S}}^T \mathbf{C} \tilde{\mathbf{S}} \, d\Omega \;\; ; \;\; \mathbf{H}^s = \int_\Omega \tilde{\mathbf{Q}}^T \mathbf{c} \tilde{\mathbf{Q}} \, d\Omega \;\; ; \\ \mathbf{G}_m^b = \int_\Omega \tilde{\mathbf{M}}^T \mathbf{B}^b \, d\Omega \;\; ; \;\; \mathbf{G}_s^b = \int_\Omega \tilde{\mathbf{S}}^T \mathbf{B}^b \, d\Omega \;\; ; \;\; \mathbf{G}^s = \int_\Omega \tilde{\mathbf{Q}}^T \mathbf{B}^s \, d\Omega \end{gathered} \tag{2.8}$$

In (2.8) $\mathbf{H}_{ss}^b$, $\mathbf{H}_{ms}^b$ and $\mathbf{G}_s^b$ reflect the effect of coupling on stress interpolations. In the absence of "loading" terms from the constitutive equations (e.g., thermal terms), the Euler-Lagrange equations may be written as:

$$\begin{bmatrix} -\mathbf{H} & \mathbf{G} \\ \mathbf{G}^T & \mathbf{0} \end{bmatrix} \begin{Bmatrix} \mathbf{n} \\ \mathbf{d} \end{Bmatrix} = \begin{Bmatrix} \mathbf{0} \\ \mathbf{f} \end{Bmatrix} \tag{2.9}$$

where

$$\mathbf{H} = \begin{bmatrix} \mathbf{H}^b_{mm} & \mathbf{H}^b_{ms} \\ \mathbf{H}^{bT}_{ms} & \mathbf{H}^b_{ss} + \mathbf{H}^s \end{bmatrix} \qquad \mathbf{G} = \begin{Bmatrix} \mathbf{G}^b_m \\ \mathbf{G}^b_s + \mathbf{G}^s \end{Bmatrix} \qquad \mathbf{n} = \begin{Bmatrix} \mathbf{m} \\ \mathbf{q} \end{Bmatrix} \tag{2.10}$$

Elimination of the stress resultant parameters for all elements gives:

$$\mathbf{K}\mathbf{d} = \mathbf{f} \tag{2.11}$$

where

$$\mathbf{K} = \mathbf{G}^T \mathbf{H}^{-1} \mathbf{G} \tag{2.12}$$

which is the stiffness matrix for the plate. Since stress resultant interpolations are independent in each element, the reduction may be performed at the element level.

3. Shear locking analysis.

Shear locking occurs at the thin plate limit when the element becomes overconstrained. As a result, bending energy becomes negligible in comparison with shear energy. In this section it is proved that elements which include coupling between the shear and moment stress resultant fields converge to the thin plate solution and do not lock in shear, provided $\mathbf{H}$ is invertible and $\mathbf{H}^b$, defined below, satisfies some rank conditions.

Throughout this section it is assumed that the stress resultant fields are given by (2.6). Furthermore, in order to satisfy the mixed patch test (Zienkiewicz, Qu, Taylor & Nakazawa [1986]), for the mixed implementation of the Reissner-Mindlin plate theory it is assumed that for all admissible boundary conditions on w, θ_x and θ_y (i.e., $\mathbf{d}_l$)

$$n_m + n_q \geq n_\theta$$

and

$$n_q \geq n_w$$

where n_q and n_m are the number of shear coefficients and moment coefficients respectively, n_θ is the number of rotational degrees of freedom, and n_w is the number of transverse displacement degrees of freedom.

To simplify notations, the following definitions are introduced :

$$\mathbf{H}^b = \mathbf{H}^{bT}_{ms} (\mathbf{H}^b_{mm})^{-1} \mathbf{H}^b_{ms} - \mathbf{H}^b_{ss}$$

and

$$\mathbf{G}^b = \mathbf{G}_m^b - \mathbf{G}_s^b$$

Proposition 3.1 : If the stress resultant fields are given by (2.6) and $\mathbf{H}^b$ and $\mathbf{H}$ are invertible, then, as thickness is reduced to zero, $\mathbf{q} = \mathbf{F}_1 \mathbf{d}$ and $\mathbf{m} = \mathbf{F}_2 \mathbf{d}$ where $\mathbf{F}_1$ and $\mathbf{F}_2$ are $O(t^3)$.

Proof : First note that $\mathbf{H}_{mm}^b$, $\mathbf{H}_{ms}^b$, $\mathbf{H}_{ss}^b$ are $O(t^{-3})$; $\mathbf{H}^s$ is $O(t^{-1})$; and $\mathbf{G}_m^b$, $\mathbf{G}_s^b$ and $\mathbf{G}^s$ are independent of t.

By (2.8), (2.9) and (2.10), $\mathbf{q}$ is given by:

$$\mathbf{q} = [\mathbf{H}^b - \mathbf{H}^s]^{-1}[\mathbf{G}^b - \mathbf{G}^s]\mathbf{d} = \mathbf{F}_1 \mathbf{d}$$

As the thickness is reduced to zero, $\mathbf{H}^s$ becomes negligible in comparison with $\mathbf{H}^b$. As a result, $\mathbf{q} = t^3 \mathbf{A}_1 \mathbf{d}$ and $\mathbf{F}_1 = t^3 \mathbf{A}_1$ where $\mathbf{A}_1$ is a matrix independent of t. Hence, $\mathbf{F}_1$ is $O(t^3)$.

By (2.8), (2.9) and (2.10), $\mathbf{m}$ is given by:

$$\mathbf{m} = (\mathbf{H}_{mm}^b)^{-1}[-\mathbf{H}_{ms}^b \mathbf{F}_1 + \mathbf{G}_m^b]\mathbf{d} = \mathbf{F}_2 \mathbf{d}$$

Consequently, $\mathbf{m} = t^3 \mathbf{A}_2 \mathbf{d}$ and $\mathbf{F}_2 = t^3 \mathbf{A}_2$ where $\mathbf{A}_2$ is a matrix independent of t. Hence, $\mathbf{F}_2$ is $O(t^3)$. ▪

Proposition 3.2 : If the stress resultant fields are given by (2.6) and $\mathbf{F}_1$ and $\mathbf{F}_2$ are $O(t^3)$, then, as thickness is reduced to zero, the shear strain energy is negligible in comparison to the bending strain energy.

Proof : By (2.7):

$$\mathbf{m}^T \mathbf{H}_{mm}^b \mathbf{m} = \mathbf{m}^T \mathbf{G}_m^b \mathbf{d} - \mathbf{m}^T \mathbf{H}_{ms}^b \mathbf{q} \tag{3.1}$$

and

$$\mathbf{q}^T \mathbf{G}_s^b \mathbf{d} = \mathbf{q}^T \mathbf{H}_{ms}^{bT} \mathbf{m} + \mathbf{q}^T \mathbf{H}_{ss}^b \mathbf{q} + \mathbf{q}^T \mathbf{H}^s \mathbf{q} - \mathbf{q}^T \mathbf{G}^s \mathbf{d} \tag{3.2}$$

The strain energy part of the Hellinger-Reissner functional (2.1) is given by:

$$\begin{aligned} \Pi_R = &-\frac{1}{2}(\mathbf{m}^T \mathbf{H}_{mm}^b \mathbf{m} + \mathbf{m}^T \mathbf{H}_{ms}^b \mathbf{q} + \mathbf{q}^T \mathbf{H}_{ms}^{bT} \mathbf{m} + \mathbf{q}^T \mathbf{H}_{ss}^b \mathbf{q} + \mathbf{q}^T \mathbf{H}^s \mathbf{q}) \\ &+ \mathbf{m}^T \mathbf{G}_m^b \mathbf{d} + \mathbf{q}^T \mathbf{G}_s^b \mathbf{d} + \mathbf{q}^T \mathbf{G}^s \mathbf{d} \end{aligned} \tag{3.3}$$

Substituting (3.1) and (3.2) into (3.3) yields:

$$\Pi_R = \frac{1}{2}(\mathbf{m}^T \mathbf{G}_m^b \mathbf{d} + \mathbf{q}^T \mathbf{H}_{ms}^{bT} \mathbf{m} + \mathbf{q}^T \mathbf{H}_{ss}^b \mathbf{q} + \mathbf{q}^T \mathbf{H}^s \mathbf{q}) \tag{3.4}$$

It follows from the assumptions that as the thickness is reduced to zero, the last term in (3.4), which

is associated with shear strain energy, is negligible compared to the first three terms, which are associated with bending strain energy. Consequently, as the thickness is reduced to zero, the shear strain energy is negligible in comparison to the bending strain energy. ▪

Proposition 3.3 : Shear locking is avoided if and only if the shear strain energy is negligible in comparison to the bending strain energy.

Proof : Assume the shear strain energy is negligible in comparison to the bending strain energy; then it follows immediately from the definition of shear locking that it does not occur.

Now assume that shear locking does not occur. Since $\overline{\mathbf{M}}$ and $\overline{\mathbf{Q}}$ are determined by equilibrium and thus are $O(t^0)$, it follows that $\mathbf{m}$ and $\mathbf{q}$ are $O(t^0)$. $\mathbf{F}_2$ is $O(t^3)$ independent of the coupling, it follows that $\mathbf{d}$ is $O(t^{-3})$. Thus, it follows from (3.4) that the shear strain energy is negligible in comparison to the bending strain energy. ▪

The restriction that $\mathbf{H}^b$ should always be invertible may be too strong. This restriction is relaxed below. As a first step spectral decomposition of $\mathbf{H}^b$ is performed.

$$\mathbf{H}^b = \mathbf{P}^T \Lambda \mathbf{P}$$

where $\mathbf{P}^T \mathbf{P} = \mathbf{I}$ the identity matrix. $\mathbf{H}^s$ is represented in the generalized coordinates ($\mathbf{P}$) as :

$$\mathbf{H}^s = \mathbf{P}^T \mathbf{P} \mathbf{H}^s \mathbf{P}^T \mathbf{P} = \mathbf{P}^T \overline{\mathbf{H}}^s \mathbf{P}$$

By (2.8), (2.9) and (2.10) :

$$(\Lambda + \overline{\mathbf{H}}^s)\,\overline{\mathbf{q}} = \overline{\mathbf{G}}\,\mathbf{d} \tag{3.5}$$

where

$$\overline{\mathbf{q}} = \mathbf{P}\mathbf{q} \qquad \overline{\mathbf{G}} = \mathbf{P}(\mathbf{G}^b - \mathbf{G}^s) \tag{3.6a}$$

$$\Lambda = \begin{bmatrix} \overline{\Lambda} & 0 \\ 0 & 0 \end{bmatrix} \qquad \overline{\mathbf{q}}^T = <\overline{\mathbf{q}}_1\ \overline{\mathbf{q}}_2> \qquad \overline{\mathbf{G}}^T = <\overline{\mathbf{G}}_1\ \overline{\mathbf{G}}_2> \tag{3.6b}$$

and

$$\overline{\mathbf{H}}^s = \begin{bmatrix} \overline{\mathbf{H}}^s_{11} & \overline{\mathbf{H}}^s_{12} \\ \overline{\mathbf{H}}^s_{21} & \overline{\mathbf{H}}^s_{22} \end{bmatrix} \tag{3.6c}$$

Substituting (3.6) into (3.5) yields:

$$\begin{bmatrix} \left(\overline{\mathbf{H}}^s_{11} + \overline{\Lambda}\right) & \overline{\mathbf{H}}^s_{12} \\ \overline{\mathbf{H}}^s_{21} & \overline{\mathbf{H}}^s_{22} \end{bmatrix} \begin{Bmatrix} \overline{\mathbf{q}}_1 \\ \overline{\mathbf{q}}_2 \end{Bmatrix} = \begin{Bmatrix} \mathbf{G}_1 \\ \mathbf{G}_2 \end{Bmatrix} \mathbf{d} \tag{3.7}$$

Let $\bar{q}_1 = \bar{F}_1 \mathbf{d}$ and $\bar{q}_2 = \bar{F}_2 \mathbf{d}$. It follows from (3.7) that $\bar{F}_1$ is $O(t^3)$ while $\bar{F}_2$ is $O(t^1)$.

Proposition 3.4 : Given that H^b is rank deficient of degree less than or equal to the maximum number of constraints allowed per element by the constraint count method (see e.g., Hughes [1987]), then $\bar{q}_2$ is $O(t^0)$.

Proof : First note that $\mathbf{d}$ is $O(t^{-3})$, as in proposition 3.3. Since $\bar{F}_1$ is $O(t^3)$, it follows that $\bar{q}_1$ is $O(t^0)$. $\bar{F}_2$ on the other hand is O(t) and so $\bar{q}_2$ is at worst $O(t^{-2})$.

As a result of meeting the constraint count requirement, shear locking does not occur. It follows from proposition 3.3 together with (3.4) that $\bar{q}$ is $O(t^\alpha)$, where $\alpha > -1$. $\bar{Q}$ is given by equilibrium, and so is $O(t^0)$. As a result, $\alpha = 0$. This result contradicts the previous result for $\bar{q}_2$.

Let $\mathbf{d} = \sum_{i=0}^{n} t^{i-3} \hat{\mathbf{d}}_i$. The above contradiction is resolved if and only if $\hat{\mathbf{d}}_0$ and $\hat{\mathbf{d}}_1$ are orthogonal to $\bar{q}_2$. As a result, $\bar{q}_2$ is $O(t^0)$. ▪

Proposition 3.5 : The vector $\bar{G}_2 \mathbf{d}$ is $O(t^{-1})$ if and only if $\bar{q}_2$ is independent of t.

Proof : This result follows immediately from (3.7) once it is noted that $\mathbf{d}$ is $O(t^{-3})$ and $\bar{q}_2$ is $O(t^0)$. ▪

Proposition 3.6 : If $\bar{Q}$ and $\bar{M}$ are $O(t^0)$ and the formulation is based on the Hellinger-Reissner functional, then the components of the shear strain tensor are $O(t^{-1})$ while the components of the curvature tensor are $O(t^{-3})$.

Proof : The Hellinger-Reissner functional may be viewed as a special case of the Hu-Washizu functional, where the assumed shear strain tensor is given by :

$$\gamma = \mathbf{c}\bar{\mathbf{Q}}$$

and the assumed curvature tensor is given by :

$$\kappa = \mathbf{C}\bar{\mathbf{M}}$$

Since both $\bar{M}$ and $\bar{Q}$ are $O(t^0)$, the desired result follows immediately. ▪

Remark 3.1 : Without the coupling between the shear and moment stress resultant fields F_1 is O(t), while F_2 is $O(t^3)$. It follows that if the coupling is neglected, then as the thickness is reduced to zero, the first three terms in (3.4), associated with bending strain energy, are negligible in

comparison to the last term, which is associated with shear strain energy. As a result, by proposition 3.3 the element locks in shear at an element level. Thus, analysis at a global level is required to determine whether shear locking occurs.

Remark 3.2 : The functional presented in (3.4) is not useful in formulating elements since the constitutive equations were used to obtain it; (3.4) can be used to obtain bounds on the strain energy.

Remark 3.3 : It follows from the above propositions that the formulation proposed in this paper guarantees elements which do not lock in shear (provided H is invertible and $\mathbf{H}^b$ is of the appropriate rank).

Remark 3.4 : It follows from proposition 3.6 that as the thickness is reduced to zero the solution obtained by the proposed formulation converges to the thin plate solution (Kirchhoff theory). It must be noted that the solution converges to the thin plate solution only when the analytical solution obtained for the Reissner-Mindlin theory converges to the thin plate solution (e.g., when point loads are considered, the thin plate solution under the load is bounded while the Reissner-Mindlin solution is not).

Remark 3.5 : As $\mathbf{H}^s$ becomes negligible(i.e., numerically zero), the mixed patch test requirement for the full recovery of $\bar{\mathbf{q}}_2$ is $n_w + n_\theta \geq n_{q2}$ where n_{q2} is the number of $\bar{\mathbf{q}}_2$ parameters. In order to maintain a robust implementation for this case $\bar{\mathbf{q}}_2$ would be taken as global variables (i.e., Lagrange multipliers). When a rectangular mesh of $n \times n$ elements, with clamped boundary conditions, is considered, the number of parameters in $\bar{\mathbf{q}}_2$ is

$$n_{q2} = \begin{cases} 2n^2 & \text{S1 element} \\ 2n\,(n+1) & \text{T1 or Bathe-Dvorkin} \\ \leq 2n^2 & \text{for elements presented in Section 4 of this paper} \end{cases}$$

and the number of displacement parameters is $n_w + n_\theta = 3(n-1)^2$ Hence, a full solution for all variables is achievable only when

$$n = \begin{cases} 6 & \text{S1 element} \\ 7 & \text{T1 or Bathe-Dvorkin} \\ \leq 6 & \text{for elements presented in Section 4 of this paper} \end{cases}$$

4. Finite element approximation.

The formulation presented in Section 2 is now used to obtain four-node quadrilateral plate elements. Accordingly, the N_I are given by the bilinear interpolation $N_I(\xi,\eta) = \frac{1}{4}(1+\xi_I\xi)(1+\eta_I\eta)$ where ξ and η are natural coordinates on the interval [-1,1] and ξ_I , η_I are the values of the natural coordinates at the node I. The assumed independent shear and moment resultant fields are presented first. Next, two options for the incompatible modes are presented leading to two elements.

4.1 Assumed resultant fields

The assumed shear and moment resultant fields are formulated in the element natural coordinates and then transformed into the physical space by means of a transformation identical to the one used to transform the second Piola-Kirchhoff stresses into Cauchy stresses. However, in order for the element to pass the patch test, the transformation is based on values at the center of the element (Pian & Sumihara [1984]).

4.1.1 Assumed Moment Resultant field.

The assumed moment resultant field is a complete linear field in the element natural coordinates and is expressed as:

$$\mathbf{M}^* = \begin{Bmatrix} M^*_{\xi\xi} \\ M^*_{\eta\eta} \\ M^*_{\xi\eta} \end{Bmatrix} = \begin{bmatrix} 1 & \xi & \eta & 0 & 0 & 0 & 0 & 0 & 0 \\ 0 & 0 & 0 & 1 & \xi & \eta & 0 & 0 & 0 \\ 0 & 0 & 0 & 0 & 0 & 0 & 1 & \xi & \eta \end{bmatrix} \begin{Bmatrix} m^*_1 \\ m^*_2 \\ \cdot \\ \cdot \\ m^*_9 \end{Bmatrix} \tag{4.1}$$

Since complete polynomials are used to express the moments, (4.1) could be used for M directly. However, the reduction to (2.6a) for satisfaction of the constraints would require selection of different parameters in each element (i.e., there would be a dependence on element orientation of ξ and η with respect to x and y). This dependence may be avoided by using the transformation procedure described next.

The following definitions are introduced:

$$xs = \frac{1}{4}\xi_I x_I \quad ; \quad xt = \frac{1}{4}\eta_I x_I \quad ; \quad xh = \frac{1}{4}(\xi\eta)_I x_I$$
$$ys = \frac{1}{4}\xi_I y_I \quad ; \quad yt = \frac{1}{4}\eta_I y_I \quad ; \quad yh = \frac{1}{4}(\xi\eta)_I y_I$$

Following Zienkiewicz [1977], the Jacobian of the coordinate transformation from (ξ, η) to (x,y) is given by :

$$J = J_0 + J_1\xi + J_2\eta$$

where,

$$J_0 = xs \cdot yt - xt \cdot ys$$
$$J_1 = xs \cdot yh - xh \cdot ys$$
$$J_2 = xh \cdot yt - xt \cdot yh$$

The resultant moments in the physical space are obtained by using the following transformation:

$$M_{ij} = \frac{1}{J_0} F_{iI} F_{jJ} M^*_{IJ}$$

where both i and j take the values x or y, and both I and J take the values ξ or η, and $F_{x\xi} = \frac{\partial x}{\partial \xi}$, etc.

At the center of the element, F is given by:

$$F_{x\xi} = xs \quad ; \quad F_{x\eta} = xt$$
$$F_{y\xi} = ys \quad ; \quad F_{y\eta} = yt$$

After redefining the independent coefficients, the assumed moment resultant field is given by :

$$\mathbf{M} = \begin{Bmatrix} M_{xx} \\ M_{yy} \\ M_{xy} \end{Bmatrix} = \begin{bmatrix} 1 & 0 & 0 & xs^2\eta & xt^2\xi & xs^2\xi & xt^2\eta & 2\,xs\,xt\,\xi & 2\,xs\,xt\,\eta \\ 0 & 1 & 0 & ys^2\eta & yt^2\xi & ys^2\xi & yt^2\eta & 2\,ys\,yt\,\xi & 2\,ys\,yt\,\eta \\ 0 & 0 & 1 & xs\,ys\,\eta & xt\,yt\,\xi & xs\,ys\,\xi & xt\,yt\,\eta & A\,\xi & A\,\eta \end{bmatrix} \begin{Bmatrix} m_1 \\ m_2 \\ \cdot \\ \cdot \\ m_9 \end{Bmatrix} \qquad (4.2)$$

where

$$A = xs\,yt + xt\,ys$$
$$m_1 = \frac{1}{J_0}(xs^2 m_1^* + xt^2 m_4^* + 2\,xs\,xt\,m_7^*)$$
$$m_2 = \frac{1}{J_0}(ys^2 m_1^* + yt^2 m_4^* + 2\,ys\,yt\,m_7^*)$$

$$m_3 = \frac{1}{J_0}\left(xs\ ys\ m_1^* + xt\ yt\ m_4^* + (xs\ yt + xt\ ys)\ m_7^* \right)$$

$$m_i = \frac{1}{J_0} m_j^*$$

with

$$(i\ ,j) \in \left\{ (4,3),(5,5),(6,2),(7,6),(8,8),(9,9) \right\}$$

It is convenient to write M in the following form:

$$\mathbf{M} = [\hat{M}_1 \mid \hat{M}_2] \begin{Bmatrix} \hat{\mathbf{m}}_1 \\ \hat{\mathbf{m}}_2 \end{Bmatrix}$$

where

$$\hat{\mathbf{m}}_1^T = < m_1 , m_2 , m_3 , m_4 , m_5 > \quad ; \quad \hat{\mathbf{m}}_2^T = < m_6 , m_7 , m_8 , m_9 >$$

with the above construction the parameter set $\hat{\mathbf{m}}_2$ may always be selected as the set to use in satisfying (2.5).

4.1.2 Assumed Shear Resultant Field.

The shear resultant field is constructed in a manner similar to that described above for M. Accordingly, let the assumed linear shear resultant field be given by:

$$\mathbf{Q}^* = \begin{Bmatrix} Q_\xi^* \\ Q_\eta^* \end{Bmatrix} = \begin{bmatrix} 1 & \xi & \eta & 0 & 0 & 0 \\ 0 & 0 & 0 & 1 & \xi & \eta \end{bmatrix} \begin{Bmatrix} q_1^* \\ q_2^* \\ \cdot \\ \cdot \\ q_6^* \end{Bmatrix} \tag{4.3}$$

The resultant shear field in the physical space is obtained by means of the following transformation :

$$Q_i = \frac{1}{J_0} F_{iI} Q_I^*$$

where i takes the values x or y and I takes the values ξ or η. After redefining the independent shear coefficients, the assumed shear resultant field in the physical space is given by:

$$\mathbf{Q} = \begin{Bmatrix} Q_x \\ Q_y \end{Bmatrix} = \begin{bmatrix} 1 & 0 & xs\,\eta & xt\,\xi & xs\,\xi & xt\,\eta \\ 0 & 1 & ys\,\eta & yt\,\xi & ys\,\xi & yt\,\eta \end{bmatrix} \begin{Bmatrix} q_1 \\ q_2 \\ \cdot \\ \cdot \\ q_6 \end{Bmatrix} \tag{4.4}$$

where

$$q_1 = \frac{1}{J_0}(xs\, q_1^* + xt\, q_4^*)$$

$$q_2 = \frac{1}{J_0}(ys\, q_1^* + yt\, q_4^*)$$

$$q_i = \frac{1}{J_0} q_j^*$$

with

$$(i,j) \in \left\{ (3,3),(4,5),(5,2),(6,6) \right\}$$

It is convenient to write Q in the following form:

$$\mathbf{Q} = [\hat{\mathbf{Q}}_1 \mid \hat{\mathbf{Q}}_2] \begin{Bmatrix} \hat{\mathbf{q}}_1 \\ \hat{\mathbf{q}}_2 \end{Bmatrix}$$

where

$$\hat{\mathbf{q}}_1^T = <q_1, q_2, q_3, q_4> \quad ; \quad \hat{\mathbf{q}}_2^T = <q_5, q_6>$$

with the above construction the parameter set $\hat{\mathbf{q}}_2$ may always be selected as the set to use in satisfying (2.5).

4.2 Assumed Incompatible Modes.

The assumed incompatible modes used in the constraint equations are presented in this section. To pass the patch test, the first derivative with respect to x and y must integrate to zero. A number of functions that satisfy this requirement are presented in the finite element literature. Here, two types of functions were chosen. The first was presented by Wu et al. [1987] and the second by Taylor et al. [1986]. While these two functions are used, they are by no means optimal.

The first type of incompatible modes used were presented by Wu et al. [1987]. The functions are given by :

$$N_1^i = \xi^2 - \frac{2J_1}{3J_0}\xi + \frac{2J_2}{3J_0}\eta \tag{4.5a}$$

$$N_2^i = \eta^2 + \frac{2J_1}{3J_0}\xi - \frac{2J_2}{3J_0}\eta \tag{4.5b}$$

The second set of the incompatible modes was presented by Taylor et al. [1986]. In order to obtain a more compact form, the incompatible modes given below are a linear combination of the modes originally presented. The functions are given by :

$$N_1^i = (1 - \frac{J_2}{J_0}\eta)(1-\xi^2) + \frac{J_1}{J_0}\xi(1-\eta^2) \tag{4.6a}$$

$$N_2^i = (1 - \frac{J_1}{J_0}\xi)(1-\eta^2) + \frac{J_2}{J_0}\eta(1-\xi^2) \tag{4.6b}$$

In order to see the difference between the functions in (4.5) and (4.6), consider the case of a constant Jacobian element. In this case, the two approaches differ by a constant. As a result, the functions presented by Taylor et al. [1986] are compatible at the nodes, while the ones presented by Pian & Wu [1987] are not. Examining the constraint equations shows the coupling term to be the only term affected by this difference.

4.3 The Elements.

Two elements are presented in this paper. The independent moment and shear resultant fields presented in (4.2) and (4.4), respectively, are used for both elements. The difference lies in the incompatible modes used in the constraint equations. The class of elements developed here is termed Coupled Resultants Bending (CRB). The element associated with the incompatible modes given by (4.5) is CRB1, while the element associated with the incompatible modes given by (4.6) is CRB2.

There are six constraint equations that are used to eliminate $\hat{\mathbf{q}}_2$ and $\hat{\mathbf{m}}_2$. The structure of the constraint equations in (2.5) implies that $\hat{\mathbf{q}}_2$ is a function of $\hat{\mathbf{q}}_1$, and $\hat{\mathbf{m}}_2$ is a function of both $\hat{\mathbf{m}}_1$ and $\hat{\mathbf{q}}_1$.

For both elements, the elastic compliances are given by:

$$\mathbf{C} = \frac{12}{E\,t^3}\begin{bmatrix} 1 & -\nu & 0 \\ -\nu & 1 & 0 \\ 0 & 0 & 2(1+\nu) \end{bmatrix} \tag{4.7}$$

for bending, and

$$\mathbf{c} = \frac{12(1+\nu)}{5E\,t}\begin{bmatrix} 1 & 0 \\ 0 & 1 \end{bmatrix} \tag{4.8}$$

for shear (Hughes [1987]) where t is the element thickness, E is Young's modulus, and ν is

Poisson's ratio. Furthermore, a shear correction factor of 5/6 has been assumed in (4.8).

5. Numerical examples.

The performance of the proposed plate elements is evaluated using a set of problems selected from the literature. The purpose of these evaluations is to test the formulation's sensitivity to the specific choice of incompatible modes as well as their overall performance. Evaluations are done with circular plates, square plates, and a highly skewed rhombic plate. Sensitivity to mesh distortion is also examined. Convergence of results is compared with the four-node selective reduced integration. Results are presented for the following elements:

CRB1 - New formulation, incompatible modes (3.5).

CRB2 - New formulation, incompatible modes (3.6).

S1 - Four-node selective reduced integration (Hughes [1987]).

Three types of boundary conditions are used :

SS1 - Simply Supported, $w = 0$, $M_s = 0$, $M_n = 0$.

SS2 - Simply Supported, $w = 0$, $\theta_s = 0$, $M_n = 0$.

Clamped - $w = 0$, $\theta_s = 0$, $\theta_n = 0$.

Convergence in the energy norm is the natural convergence test for the finite element method (Strang & Fix [1973]). It is common practice in the literature, however, to examine convergence of the finite element solution by analyzing the displacements at characteristic points. In this paper, convergence is examined in terms of both energy norm and center displacement (strain energy reported is twice the internal strain energy). All tables and figures show the center displacement/energy norm as a function of the number of elements (denoted nel) used in the corresponding mesh.

5.1 Circular Plates.

A circular plate is modeled using 3, 12, 48 and 192 elements. Due to symmetry, only one quadrant is discretized. A typical mesh is shown in Figure 5.1. While the three-element mesh results are retained, it should be noted that significant errors result in approximating the domain. SS1 and

clamped boundary conditions are reported.

Material Properties				
	E	ν	t	R
Thin Plate	10920	0.3	0.1	5.0
Thick Plate	1.365	0.3	2.0	5.0

These properties indicate that the plate stiffness $D = \frac{E\,t^3}{12(1-\nu^2)} = 1.0$.

Two loading types are examined: (1) Uniform transverse unit load and (2) Unit point load at the center of the plate.

5.1.1 Uniform Transverse Unit Load.

Results are compared with the analytical solution. In case of a clamped boundary, the center transverse displacement is given by:

$$w(0) = \frac{q\,R^4}{64D}\left[1 + \frac{8}{3\kappa(1-\nu)}\left(\frac{t}{R}\right)^2\right]$$

and the strain energy is given by:

$$E_{CL} = \frac{q^2 R^6 \phi}{384D}\left[1 + \frac{4}{\kappa(1-\nu)}\left(\frac{t}{R}\right)^2\right]$$

ϕ is the sector analyzed, and is equal to $\frac{\pi}{2}$ in the present examples. For the simply supported case, the center transverse displacement is given by:

$$w(0) = \frac{q\,R^4}{64D}\left[\frac{5+\nu}{1+\nu} + \frac{8}{3\kappa(1-\nu)}\left(\frac{t}{R}\right)^2\right]$$

and the strain energy is given by:

$$E_{SS} = \frac{q^2 R^6 \phi}{384D}\left[\frac{7+\nu}{1+\nu} + \frac{4}{\kappa(1-\nu)}\left(\frac{t}{R}\right)^2\right]$$

$\kappa = \frac{5}{6}$ for all examples. It should again be noted that the above energy expressions represent the total work by the external transverse loads and thus are twice the actual strain energy.

Simply supported thin plate.

Results for SS1 boundary conditions are summarized in Table 5.1 and shown in Figure 5.2. The exact solutions are $w = 39.83156$ and $E_{SS} = 359.08748$.

Table 5.1 Circular Plate - Uniform load, SS1, t = 0.1

nel	CRB1		CRB2		S1	
	disp.	energy	disp.	energy	disp.	energy
3	33.42998	244.54439	36.50937	282.52226	30.22337	210.01115
12	38.25803	327.44936	39.37985	345.96120	37.06431	314.57406
48	39.49348	351.18592	39.84320	356.66770	39.13917	347.41788
192	39.74969	357.11690	39.84496	358.55001	39.65848	356.14125

Monotonic convergence is obtained for all three elements in both the energy norm and the center displacement. The CRB2 element shows a clear superiority over the other two elements reported. With only three elements in the mesh, 78.7% of the exact strain energy and 91.7% of the exact center transverse displacement is obtained.

Clamped thin plate.

Results for a clamped boundary are summarized in Table 5.2 and shown in Figure 5.3. The exact solutions are $w = 9.78348$ and $E_{CL} = 64.09118$.

Monotonic convergence in both the energy norm and center displacement is obtained in the case of all elements. Both the CRB1 and CRB2 elements converge from above for the clamped boundary, while for SS1 boundary conditions, convergence was from below. The CRB2 element, which performed well for the SS1 boundary conditions, yields very flexible results for this example: 177.7% of the exact energy for three elements and 136.1% for twelve elements. However, error analysis on the results shows that quadratic rate of convergence in energy is obtained. The CRB1 element yields the best result for this problem. With twelve elements in the mesh, 106.8% of the exact strain energy and 104.7% of the center transverse displacement is obtained.

Table 5.2 Circular Plate - Uniform load, Clamped, t = 0.1

nel	CRB1		CRB2		S1	
	disp.	energy	disp.	energy	disp.	energy
3	11.07388	70.40178	15.36831	113.87654	7.18244	33.69067
12	10.24633	68.44072	11.60705	87.22176	8.93063	54.09140
48	9.92960	65.43534	10.29889	70.86546	9.57239	61.67277
192	9.82260	64.44775	9.91879	65.85591	9.73120	63.4829

Simply supported thick plate.

Results are summarized in Table 5.3 and shown in Figure 5.4. The exact solutions are $w = 46.95656$ and $E_{SS} = 429.03701$.

Table 5.3 Circular Plate - Uniform load, SS1, t = 2.

nel	CRB1		CRB2		S1	
	disp.	energy	disp.	energy	disp.	energy
3	41.22420	298.80969	44.35011	336.93226	36.98856	261.32771
12	45.52658	393.25690	46.85908	412.18318	44.07056	379.42456
48	46.59817	419.89374	46.97144	425.41230	46.23842	416.07601
192	46.86700	426.73833	46.96275	428.17104	46.77711	425.76041

Monotonic convergence in the energy norm is obtained for all three elements. However, in terms of the center transverse displacement, the CRB2 element does not converge monotonically. This illustrates the difficulty of comparing solutions at a single point and why energy is the more natural basis for comparison. As in the case of the simply supported thin plate, convergence is obtained from below and the CRB2 element yields the best results. With only three elements, 78.5% of the exact energy and 94.4% of the exact center transverse displacement is obtained. When a twelve element mesh is used, 99.8% of the exact center transverse displacement and 96.1% of the exact strain energy is obtained for the CRB2 element.

Clamped thick plate.

Results are summarized in Table 5.4 and shown in Figure 5.5. The exact solutions evaluated from the above are $w = 16.90848$ and $E_{CL} = 134.04070$.

Table 5.4 Circular Plate - Uniform load, Clamped, t = 2.

nel	CRB1		CRB2		S1	
	disp.	energy	disp.	energy	disp.	energy
3	18.29822	123.25616	21.87458	165.41479	13.85127	85.09326
12	17.36156	133.54089	18.73937	152.52507	15.94038	119.79678
48	17.02945	134.10303	17.40752	139.54992	16.67009	130.33612
192	16.93933	134.06845	17.03586	135.47738	16.84915	133.10516

Monotonic convergence in both the energy norm and center transverse displacement is obtained for CRB2 and S1 elements. The CRB1 element converges monotonically only in center displacement. Both the CRB1 and CRB2 elements converge from above in terms of the center

transverse displacement. However, the CRB1 element converges from below in the energy norm, while the CRB2 converges from above. As in the clamped thin plate, the CRB2 element is too flexible for coarse meshes. The CRB1 element again yields excellent results for the clamped problem. With only three elements, 92.0% of the strain energy and 108.2% of the center transverse displacement is obtained.

5.1.2 Concentrated Transverse Unit Load at the Center.

The case of a unit point loading yields a strain energy equal to the displacement under the load and therefore, the strain energy need not be reported. In the thick plate case, the exact center transverse displacement is infinite. The finite element method however, because it is a weak approximation, gives a finite displacement. This example is included to test the sensitivity of the formulation to singularity in the solution.

Simply supported thin and thick plates.

Results for simply supported plates are summarized in Table 5.5 and shown in Figures 5.6 (thin plate) and 5.7 (thick plate). The exact displacement at the center for the thin plate is $w = 1.26253$ (Timoshenko & Woinowsky-Krieger [1959]). As noted above the displacement at the center for the thick plate solution is infinite (due to shear deformation).

Table 5.5 Circular Plate - Point load, SS1

nel	t = .1			t = 2.		
	CRB1	CRB2	S1	CRB1	CRB2	S1
3	1.23384	1.41495	1.24773	1.87239	2.04916	1.93862
12	1.25908	1.31392	1.22777	1.94858	2.03346	2.17221
48	1.27140	1.29140	1.25529	2.04870	2.07849	2.44954
192	1.26863	1.27617	1.26347	2.16517	2.17449	2.70885

Monotonic convergence for all three elements is obtained for the thick plate case. When rate of convergence for the thick plate is examined, the best result is obtained by the S1 element. This is due to the singularity of this element as will be shown in the next example. In the thin plate case, results for the CRB2 and S1 elements converge monotonically while results for CRB1 element do not.

Clamped thin and thick plates.

The results for both thin and thick plates are summarized in Table 5.6 and shown in Figure 5.8 (thin plate) and Figure 5.9 (thick plate).

Table 5.6 Circular Plate - Point load, Clamped

nel	t = .1			t = 2.		
	CRB1	CRB2	S1	CRB1	CRB2	S1
3	0.51034	0.66957	0.42038	1.13124	1.34436	1.16862
12	0.50512	0.55652	0.46327	1.19051	1.28218	1.44900
48	0.50799	0.52902	0.49040	1.28538	1.31671	1.72465
192	0.50385	0.51168	0.50316	1.40055	1.41022	1.98356

Monotonic convergence in the thin plate case is obtained for the CRB2 and S1 elements, but not for CRB1 . In the thick plate case however, all three elements show monotonic convergence.

The thick plate case is used next to demonstrate the stability of the new formulation. The transverse displacements along the radius, for a mesh with 48 elements, are summarized in Table 5.7 and exhibits in Figure 5.10. The exact solution can be found in Lukasiewicz [1979]. The S1 element shows a known instability (Hughes [1987]). On the other hand, the CRB1 and CRB2 elements produce excellent results.

Table 5.7 Thick clamped circular plate, transverse displacements along the radius.

r	CRB1	CRB2	S1	EXACT
0.	1.28538	1.31671	1.72465	∞
0.625	0.82288	0.84102	0.42266	0.77877
1.25	0.63154	0.64307	0.90043	0.59442
1.875	0.46784	0.47606	0.23844	0.44186
2.5	0.32564	0.33267	0.49660	0.30781
3.125	0.20610	0.21212	0.05851	0.19312
3.75	0.10956	0.11407	0.20740	0.10111
4.375	0.03979	0.04229	-0.01478	0.03552
5.	0.	0.	0.	0.

5.2 Square Plates.

A square plate is modeled using meshes of uniform square elements. Due to symmetry, only one quadrant is discretized, and a typical mesh is shown in Figure 5.11.

Material Properties				
	E	ν	t	L
Thin Plate	10.92E+6	0.3	0.01	5.0
Thick Plate	1.365	0.3	2.0	5.0

Using these properties, the plate bending stiffness D = 1.0.

Only the case of uniform loading is examined. The boundary conditions examined are : SS1, SS2 and clamped.

The "exact" energy reported is computed from:

$$E = \int_{\Omega} q(x,y)\, w(x,y)\, d\Omega$$

using a Fourier series solution and, thus, is twice the actual strain energy.

5.2.1 Thin Plate.

Results are compared to an analytical solution (in a series form) given by Timoshenko & Woinowsky-Krieger [1959]. In the case of a simply supported plate, analytical results are given only for SS2 boundary conditions.

Simply supported plate.

Results for a thin plate with SS1 and SS2 boundary conditions are summarized in Tables 5.8 and 5.9, respectively, and shown in Figure 5.12. The exact solution is $w = 40.623$ and $E = 425.6276$.

Table 5.8 Square Plate - Uniform load, SS1, t = 0.01

nel	CRB1		CRB2		S1	
	disp.	energy	disp.	energy	disp.	energy
1	49.89058	311.81615	39.00275	243.76716	60.09651	375.60319
4	42.82542	398.80376	42.24268	389.90478	43.24200	402.47456
16	41.14819	418.93874	40.95346	418.30261	41.28000	419.80500
64	40.77255	424.12572	40.71770	424.07838	40.78936	424.20080
256	40.70100	425.63930	40.68911	425.69397	40.67196	425.35466

Monotonic convergence is obtained for all three elements in the energy norm for the SS1 boundary condition. With the exception of the one element mesh, the three elements yield almost identical results.

Table 5.9 Square Plate - Uniform load, SS2, t = 0.01

nel	CRB1		CRB2		S1	
	disp.	energy	disp.	energy	disp.	energy
1	31.89756	199.35976	31.89659	199.35372	31.88811	199.30070
4	39.69936	364.09940	39.69458	364.05563	39.69009	364.00955
16	40.44459	410.13559	40.42559	409.94346	40.41444	409.80934
64	40.66742	422.70231	40.61320	422.15320	40.57234	421.64838
256	40.69900	425.62046	40.69314	425.65472	40.61095	424.63303

For the SS2 boundary condition, monotonic convergence in both the energy norm and center transverse displacement is obtained for all three elements. Again the three elements yield almost identical results.

Clamped plate.

Results are summarized in Table 5.10 and shown in Figure 5.13. The thin plate solution is $w = 12.6$ (Timoshenko & Woinowsky-Krieger [1959]).

Table 5.10 Square Plate - Uniform load, Clamped, t = 0.01

nel	CRB1		CRB2		S1	
	disp.	energy	disp.	energy	disp.	energy
1	0.00011	0.00670	0.00011	0.00670	0.00004	0.00223
4	12.11830	75.75949	12.11691	75.75084	12.11266	75.70555
16	12.52712	91.88611	12.52163	91.84711	12.50715	91.66355
64	12.68109	96.59564	12.67157	96.57340	12.61672	95.86400
256	12.70854	97.63482	12.75608	98.36972	12.64424	96.92734

All three elements yield nearly identical results (if results for one-element mesh are ignored). With only four-element mesh, 96.0% of the exact center transverse displacement is obtained.

It is noted that all three elements lock when the one-element mesh is used. This is expected since all rotational degrees-of-freedom are constrained and thus rotations are identically zero. Under these constraints, for thin plates where shear deformations are negligible, the derivatives of the transverse displacement are negligible. As a result, the transverse displacement tends to zero as the plate thickness approaches zero.

5.2.2 Thick Plates.

Simply supported plate.

Results for SS1 and SS2 boundary conditions are summarized in Tables 5.11 and 5.12 respectively, and shown in Figure 5.14. While convergence is obtained in both cases, it is of interest to note that the converged solution for SS1 boundary condition is about 13% higher in both the energy norm and the center transverse displacement than results using the SS2 restraints.

Table 5.11 Square Plate - Uniform load, SS1, t = 2.

nel	CRB1		CRB2		S1	
	disp.	energy	disp.	energy	disp.	energy
1	63.99719	399.98244	57.54543	359.65891	74.38187	464.88668
4	58.61877	551.24726	61.82475	595.31737	56.54353	538.24175
16	55.96186	585.20271	57.76508	610.13517	55.65013	584.16547
64	55.52584	596.38017	56.07810	604.04344	55.49343	596.64229
256	55.46432	599.72511	55.61035	601.75198	55.46040	599.83988

The analytical solution for SS2 boundary condition (series solution which includes shear deformation) is $w = 49.043$ and $E = 526.04$.

Table 5.12 Square Plate - Uniform load, SS2, t = 2.

nel	CRB1		CRB2		S1	
	disp.	energy	disp.	energy	disp.	energy
1	61.73804	385.86275	56.57157	353.57232	46.17347	288.58418
4	55.36514	522.66899	57.53090	552.09748	49.21366	460.73333
16	50.65914	526.73375	51.39402	537.55077	49.05768	509.26852
64	49.44576	526.29476	49.63552	529.14510	49.04449	521.81896
256	49.14365	526.10835	49.19135	526.82857	49.04333	524.98282

Monotonic convergence in the energy norm is obtained only for the S1 element. The CRB1 yields excellent results, with only four elements in the mesh, 99.4% of the exact strain energy and 112.9% of the center transverse displacement is obtained.

Clamped plate.

Results are summarized in Table 5.13 and shown in Figure 5.15. The S1 element yields the best results among the three elements considered. Both the CRB1 and CRB2 elements yield flexible results. However, the CRB1 element is just slightly flexible for the coarse meshes, 116.7% of the result obtained for 256 elements while the CRB2 is very flexible, 152% of the result obtained for 256

elements (the four-element mesh results are used).

Table 5.13 Square Plate - Uniform load, Clamped, t = 2.

nel	CRB1		CRB2		S1	
	disp.	energy	disp.	energy	disp.	energy
1	20.52723	128.29521	31.20194	195.01214	14.28571	89.28571
4	25.45333	215.82077	32.89409	300.06833	21.77378	176.36950
16	22.84967	208.66491	24.84375	234.74044	21.73858	196.77579
64	22.01024	205.08661	22.51119	211.82512	21.72456	201.99788
256	21.79410	204.09345	21.91939	205.79011	21.72225	203.31405

5.3 Rhombic Plate.

A simply supported rhombic plate of side a = 100, material properties E = 10E+6, ν = 0.3 and t = 1.0 is loaded by a unit uniform loading. A typical mesh used is shown in Figure 5.16. Results are summarized in Table 5.14 and shown in Figure 5.17. A comparison solution of 0.04455 has been obtained by Morely [1963].

Table 5.14 Rhombic Plate - Uniform load, SS1, t = 1., a = 100., Θ=30°

nel	CRB1		CRB2		S1	
	disp.	energy	disp.	energy	disp.	energy
4	0.04031	50.38521	0.07143	89.28845	0.02932	36.64600
16	0.04150	64.76201	0.04724	72.14388	0.04509	66.60848
64	0.04304	72.32353	0.04538	76.54601	0.04438	72.56578
256	0.04456	76.33087	0.04620	79.00726	0.04482	76.30679
1024	0.04535	78.06687	0.04645	79.64557	0.04561	78.33507

The difficulty of this problem is due to the singularity of the solution for the moments and shears at the obtuse vertices. Monotonic convergence in both the energy norm and the center transverse displacement is obtained for both the CRB1 and S1 elements.

5.4 Mesh Distortion.

To study the sensitivity to mesh distortion, a coarse mesh modeling a clamped square plate is used. Only four elements are used to model one quadrant of the plate. Material properties are as for the thin square plate example. Two types of distortions are introduced. First, the center node of the mesh is moved along the main diagonal of the plate as shown in Figure 5.18. Results are summarized in Table 5.15, and shown in Figure 5.19.

Table 5.15 Mesh Distortion - Symmetric			
Δ	CRB1	CRB2	S1
-1.25	13.81498	24.22608	11.05384
-1.00	13.90309	19.35489	11.60235
-0.50	12.46806	12.84389	12.09558
0.00	12.11830	12.11691	12.11266
0.50	13.47277	13.31214	11.65238
1.00	13.43153	16.46809	10.59494
1.25	12.62252	19.47493	9.74557

The CRB2 becomes flexible as the mesh is distorted. The CRB1 on the other hand, is flexible for the initial distortion and stiffens as the mesh is further distorted. None of the three elements produce results that lock in shear.

Next, the center node is moved parallel to the edge as shown in Figure 5.20. Results are summarized in Table 5.16 and shown in Figure 5.21.

Table 5.16 Mesh Distortion - Asymmetric			
Δ	CRB1	CRB2	S1
0.00	12.11830	12.11691	12.11266
0.02	11.65779	11.65193	11.96376
0.04	10.74749	10.73900	11.54479
0.06	9.98084	9.97098	10.90864
0.08	9.47010	9.45938	10.12638
0.10	9.14943	9.13807	9.26993
0.15	8.78086	8.76871	7.15812
0.20	8.67658	8.66506	5.41817
0.30	8.71685	8.71264	3.18270
0.50	9.07152	9.12362	1.35339
0.80	9.72854	10.08500	0.55073
1.00	10.09830	10.93894	0.35102
1.50	10.07783	13.89768	0.15030
2.00	7.66371	16.95343	0.08055
2.49	4.25383	19.67465	0.04951

The difficulty of this mesh is that there are only eight degrees-of-freedom. Thus, shear locking becomes an important issue as the symmetry of the mesh is lost. Results show both CRB1 and CRB2 elements do not lock in shear while the S1 does. This locking is dependent on the plate thickness. Numerical results indicate that severe locking occurs as the distortion becomes larger than about twelve times the plate thickness. Thus, as the thickness is reduced, the S1 element becomes more and more sensitive to mesh distortion. The CRB1 and CRB2 elements, on the other hand, do not lock but show a faster deterioration than the S1 element in the initial distortion phase, as is evident form Figure 5.21.

6. Concluding Remarks.

This paper has introduced a mixed formulation for plate bending finite elements based upon the Reissner-Mindlin plate theory. Starting from the Hellinger-Reissner functional, the terms associated with incompatible displacements were forced to vanish. As a result, constraint equations on the shear and moment stress resultant fields were introduced. Because of these constraint equations, a coupling term between the assumed independent shear and moment stress resultant fields was introduced.

As a result of the explicit coupling between the shear and moment stress resultant fields, the resulting elements are free of shear locking and possess the correct rank, as proved and demonstrated by the numerical results. Thus, without resorting to ad-hoc assumptions, elements free of shear locking can be obtained. The coupling term introduced is consistent with the Reissner-Mindlin plate theory as is evident from the structure of the equilibrium equations.

Both the CRB1 and CRB2 elements presented in this paper yield good results for both thin and thick plates. While flexible in the thick plate cases, rapid convergence was obtained. The mesh distortion test introduced in this paper shows the new formulation to be free of shear locking, even when the S1 element locks in shear.

The remaining open question is how to choose the incompatible modes. As is illustrated in this paper, the resulting element performance is heavily dependent upon the choice of the incompatible modes. In this paper, the incompatible displacements were selected so that the resulting elements would satisfy the patch test requirements. The objective was to show that the proposed formulation leads to elements of the correct rank and free of shear locking. The question of optimal conditions for the incompatible modes is left for future research.

Acknowledgments

We wish to thank Professor J. Lubliner, Mr. M. Jamjian and Mr. N. Tarnow for many helpful discussions. The help of Mr. P.L.M. Van Roy in producing the figures is appreciated.

REFERENCES

Bathe, K.J. & E.N. Dvorkin, [1984], "A Continuum Mechanics Based Four-Node Shell Element for General Non-Linear Analysis," *International Journal for Computer-Aided Engineering and*

Software, Vol. 1, pp. 77-88.

Hughes, T.J.R. & T.E. Tezduyar, [1981], "Finite Elements Based Upon Mindlin Plate Theory with Particular Reference to the Four Node Bilinear Isoparametric Element," *Journal of Applied Mechanics,* Vol. 46, pp. 587-596.

Hughes, T.J.R., [1987], *The Finite Element Method,* Prentice-Hall, Inc., Englewood Cliffs, New Jersey.

Lukasieicz, S., [1979], *"Local Loads in Plates and Shells",* Sijthoff & Noordhoff, the Netherlands.

Malkus, D.S. & T.J.R. Hughes, [1978], "Mixed Finite Element Methods - Reduced and Selective Integration Techniques: A Unification of Concepts", *Computer Methods in Applied Mechanics and Engineering,* Vol. 15, No. 1, pp. 63-81.

Morley, L.S.D., [1963], "Skew Plates and Structures", *International Series of Monographs in Aeronautics and Astronautics,* New York.

Pawsey, S.F. &R.W. Clough, [1971], "Improved Numerical Integration for Thick Slab Finite Elements," *International Journal for Numerical Methods in Engineering,* Vol. 3, pp. 575-586.

Pian, T.H.H. & K. Sumihara, [1984], "Rational Approach for Assumed Stress Finite Elements", *International Journal for Numerical Methods in Engineering,* Vol. 20, pp. 1685-1695.

Pian, T.H.H. & C.-C. Wu, [1988], "A Rational Approach for Choosing Stress Terms for Hybrid Finite Element Formulations", *International Journal for Numerical Methods in Engineering,* Vol. 26, pp. 2331-2343.

Strang, G. & G.J. Fix, [1973], *An Analysis of the Finite Element Method,* Prentice-Hall, Inc., Englewood Cliffs, New Jersey.

Taylor, R.L., O.C. Zienkiewicz, J.C. Simo & A.H.C. Chan, [1986], "The Patch Test for Mixed Formulations", *International Journal for Numerical Methods in Engineering,* Vol. 22, pp. 32-62.

Timoshenko, S. & S. Woinowsky-Krieger, [1959], *Theory of Plates and Shells,* McGraw-Hill, New York.

Wu, C.-C., M.-G. Huang & T.H.H. Pian, [1987], "Consistency Condition and Convergence Criteria of Incompatible Elements: General Formulation of Incompatible Functions and its Application", *Computers & Structures,* Vol. 27, No. 5, pp. 639-644.

Zienkiewicz, O.C., [1977], *The Finite Element Method,* 3rd ed., MacGraw-Hill Book Co., London.

Zienkiewicz, O.C., S. Qu, R.L. Taylor & S. Nakazawa, [1986], "The Patch Test for Mixed Formulations", *International Journal for Numerical Methods in Engineering,* Vol. 23, pp. 1873-1883.

Zienkiewicz, O.C., R.L. Taylor & J. Too, [1971], "Reduced Integration Technique in General Analysis of Plates and Shells", *International Journal for Numerical Methods in Engineering,* Vol. 3, pp. 275-290.

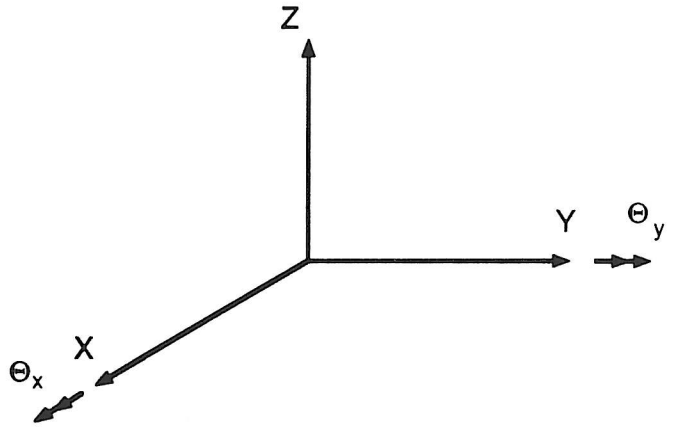

Figure 2.1 - Sign conventions for rotations, right-hand-rule rotations.

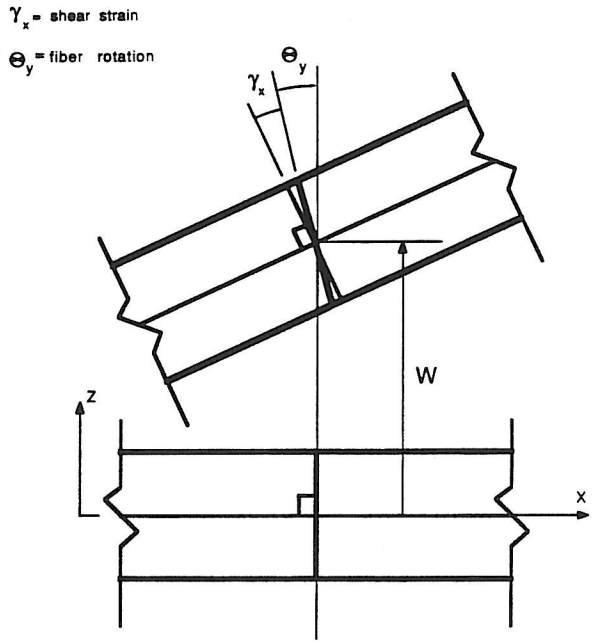

Figure 2.2 - Plate kinematics.

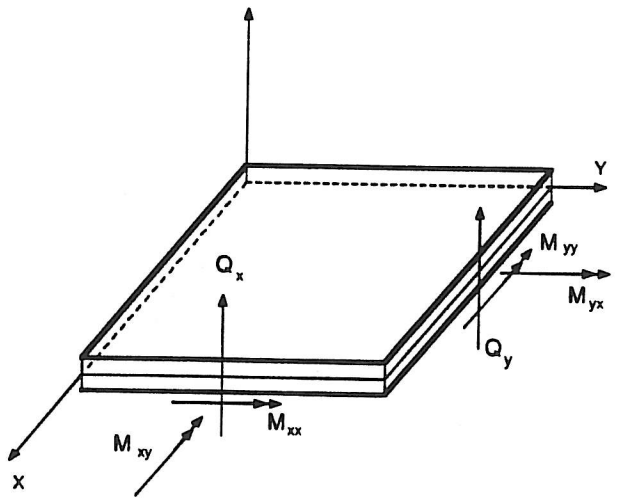

Figure 2.3 - Sign conventions for stress resultants on positive faces.

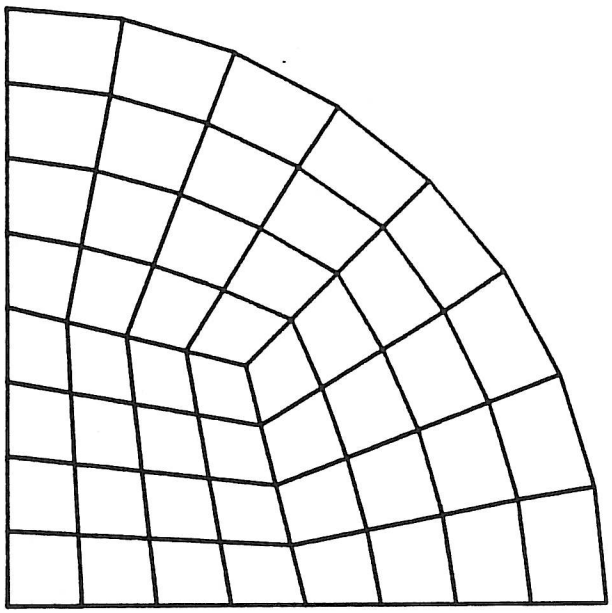

Figure 5.1 - Circular plate. Due to symmetry only one quadrant is discretized.

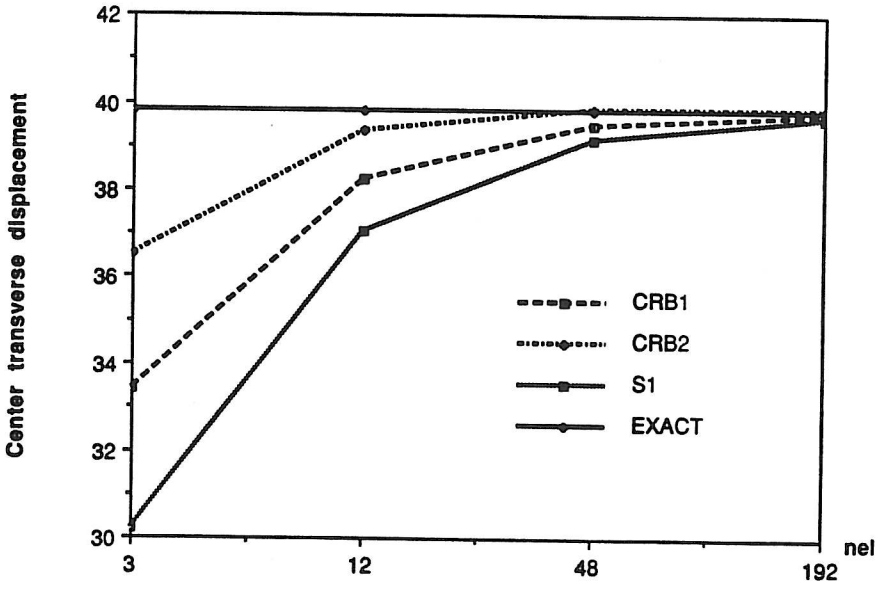

Figure 5.2 - Convergence study for thin circular plate; simply supported, uniform load.

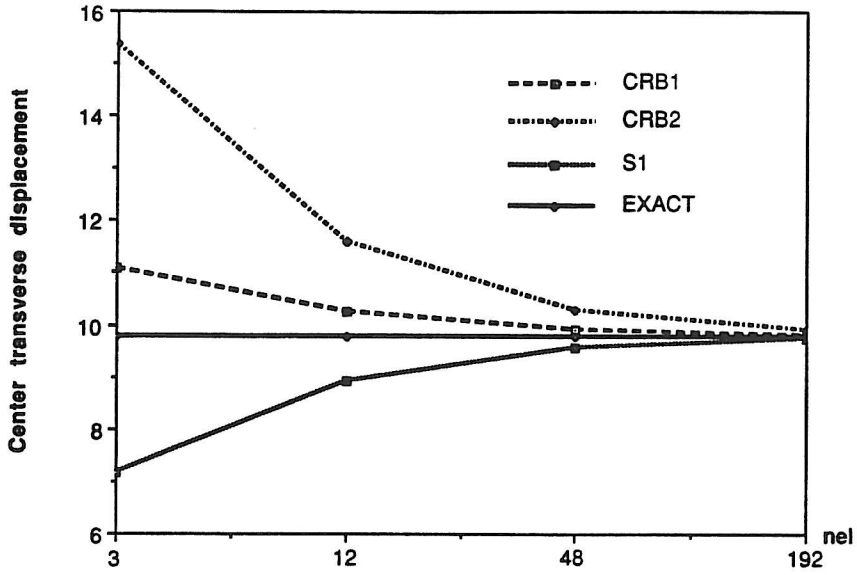

Figure 5.3 - Convergence study for thin circular plate; clamped, uniform load.

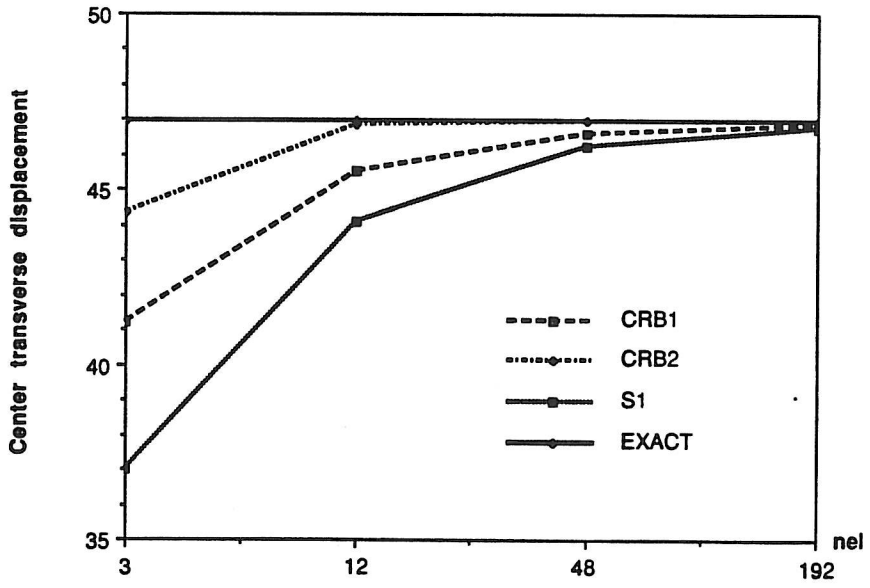

Figure 5.4 - Convergence study for thick circular plate; simply supported, uniform load.

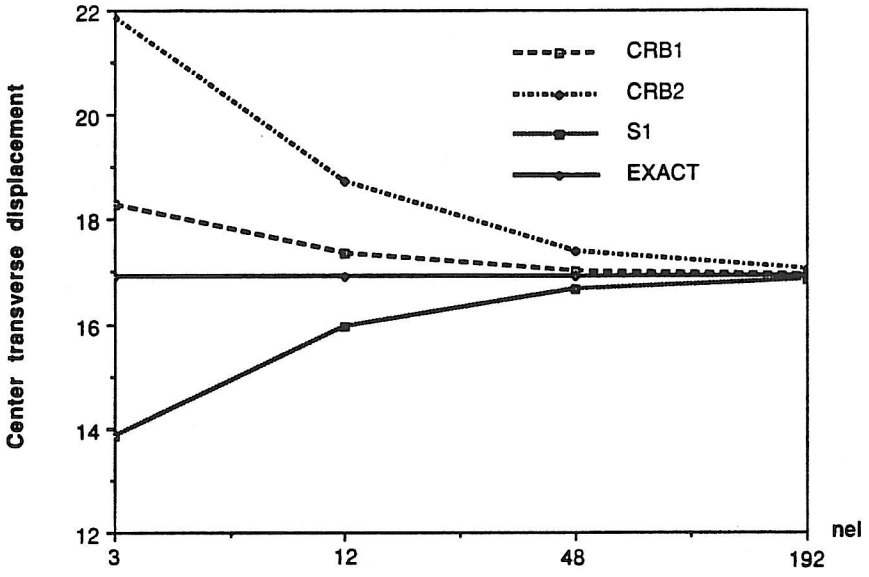

Figure 5.5 - Convergence study for thick plate; clamped, uniform load.

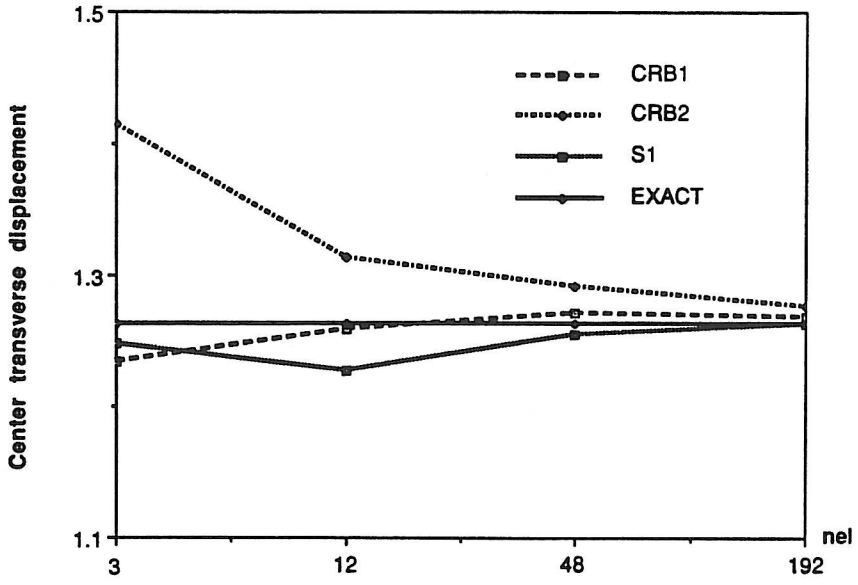

Figure 5.6 - Convergence study for thin circular plate; simply supported, concentrated load.

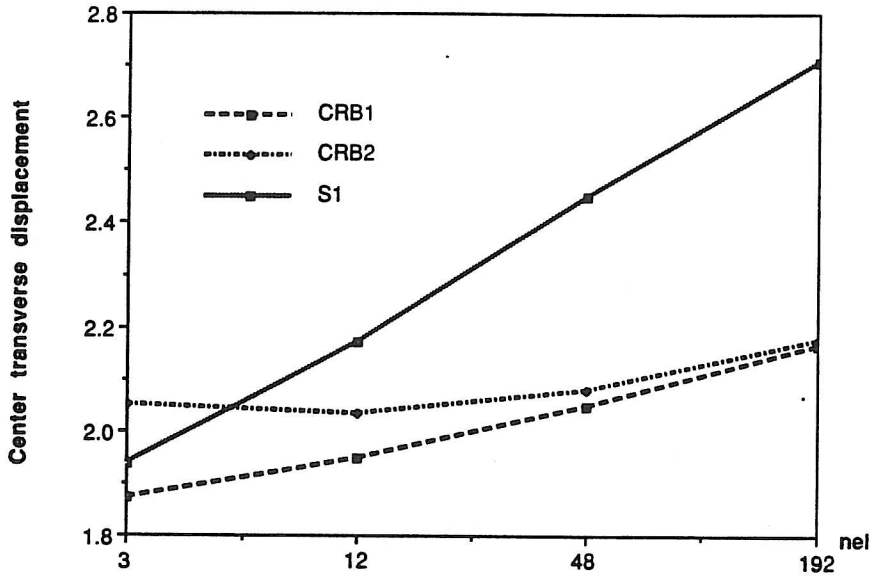

Figure 5.7 - Thick circular plate; simply supported, concentrated load.

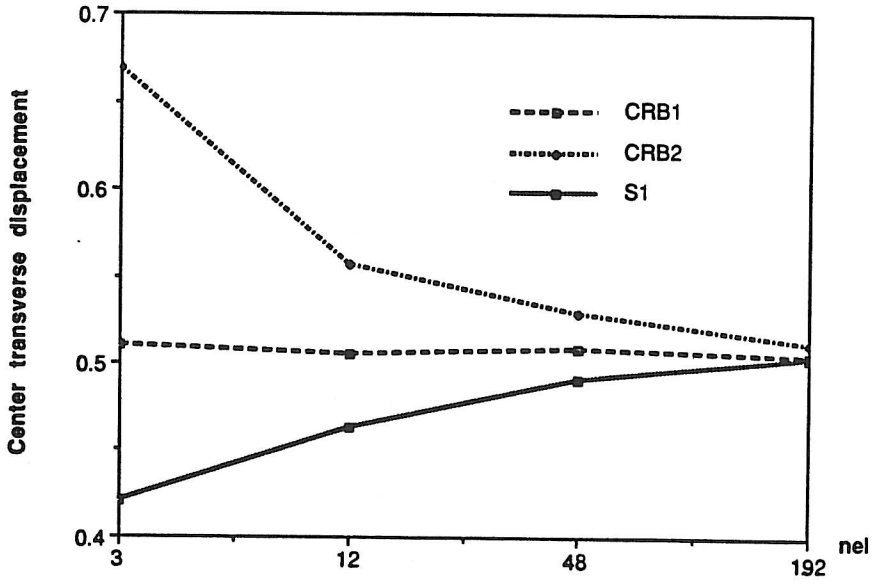

Figure 5.8 - Thin circular plate; clamped, concentrated load.

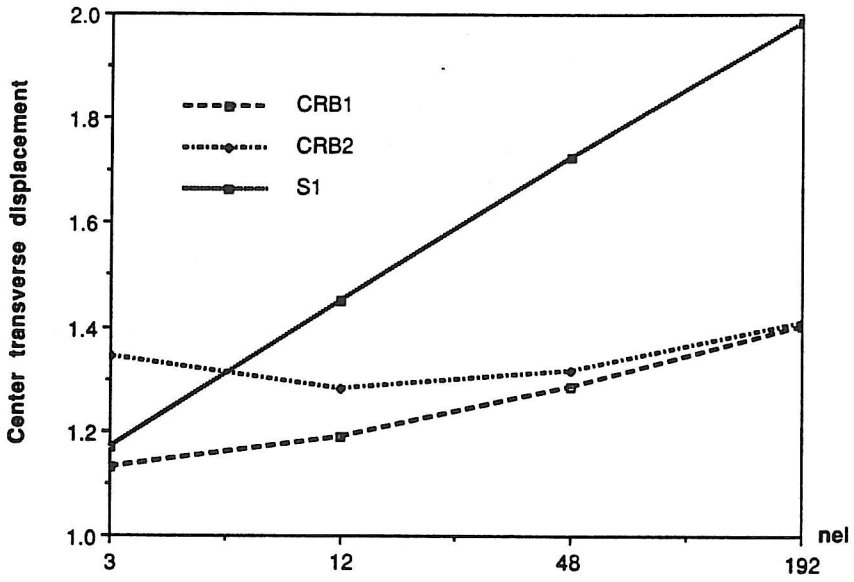

Figure 5.9 - Thick circular plate; clamped, concentrated load.

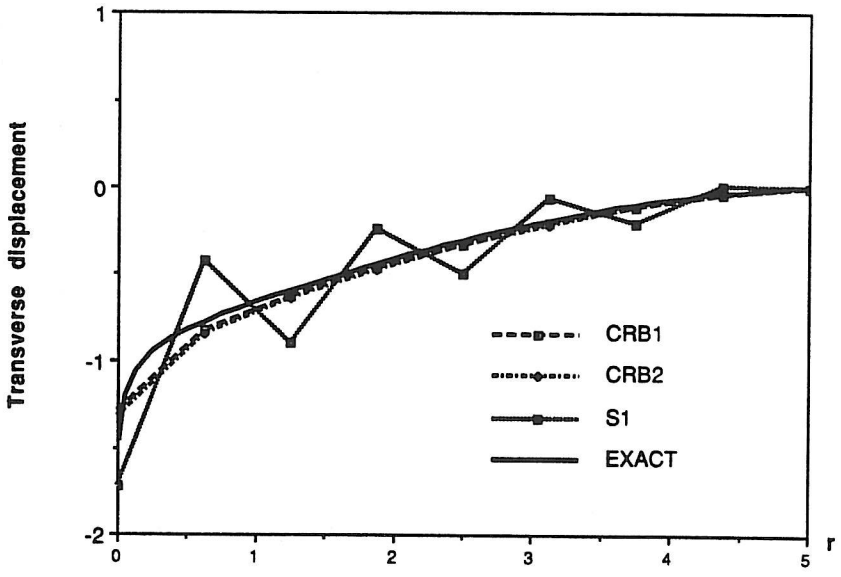

Figure 5.10 - Transverse displacement along the radius; clamped thick circular plate.

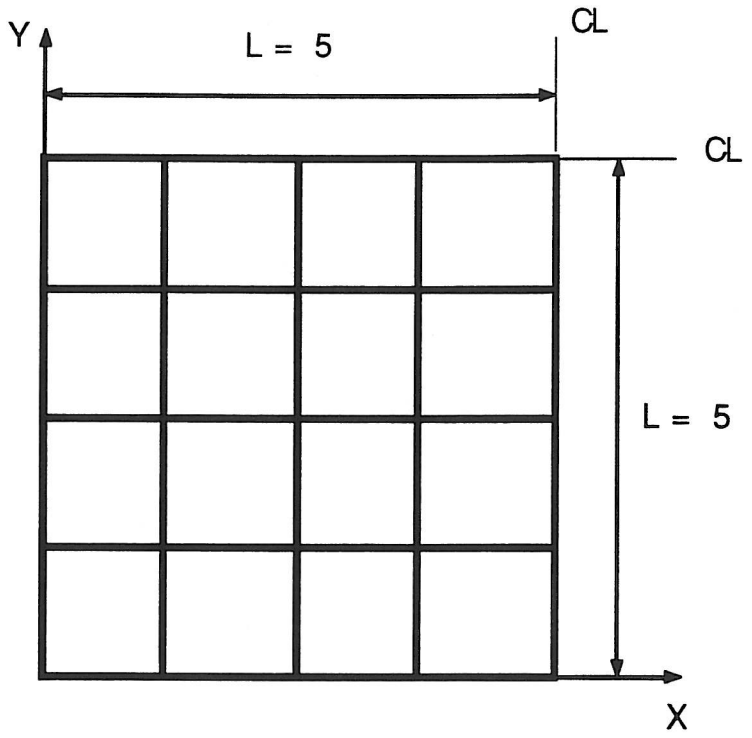

Figure 5.11 - Square plate. Due to symmetry only one quadrant is discretized.

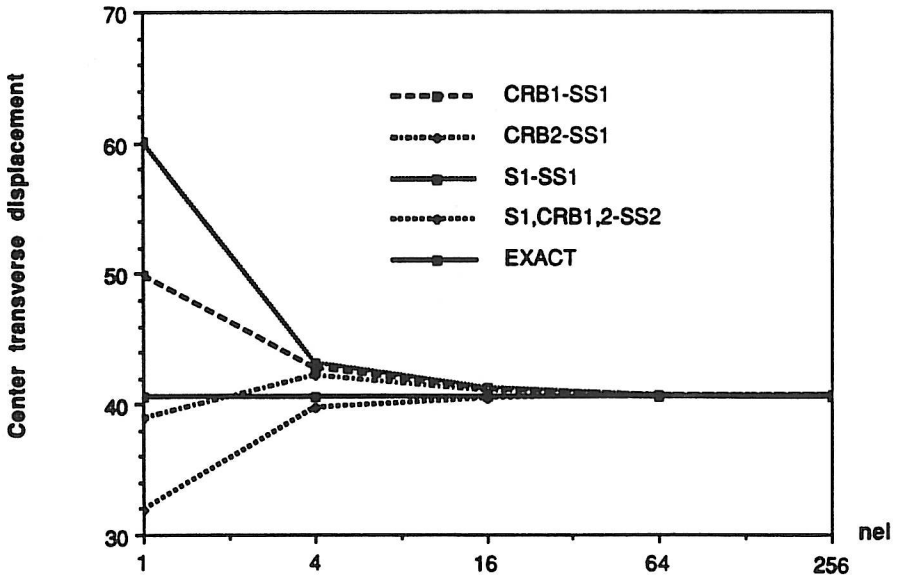

Figure 5.12 - Convergence study for thin square plate, simply supported.

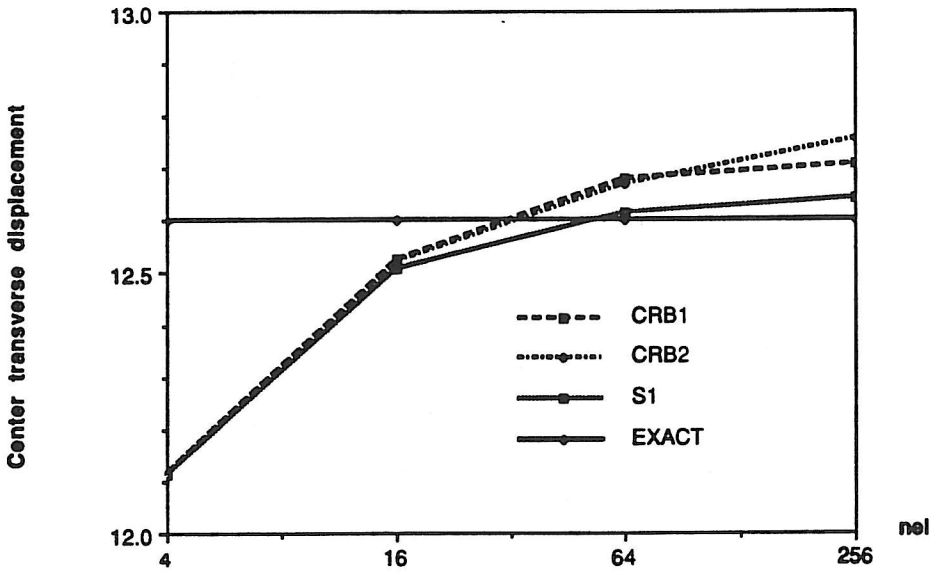

Figure 5.13 - Convergence study for thin square plate, clamped.

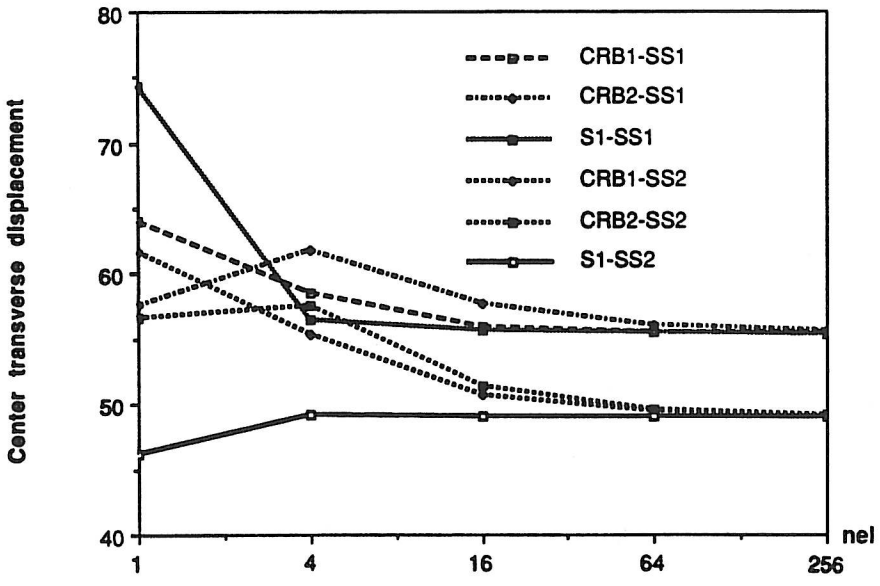

Figure 5.14 - Convergence study for thick square plate; simply supported, uniform load.

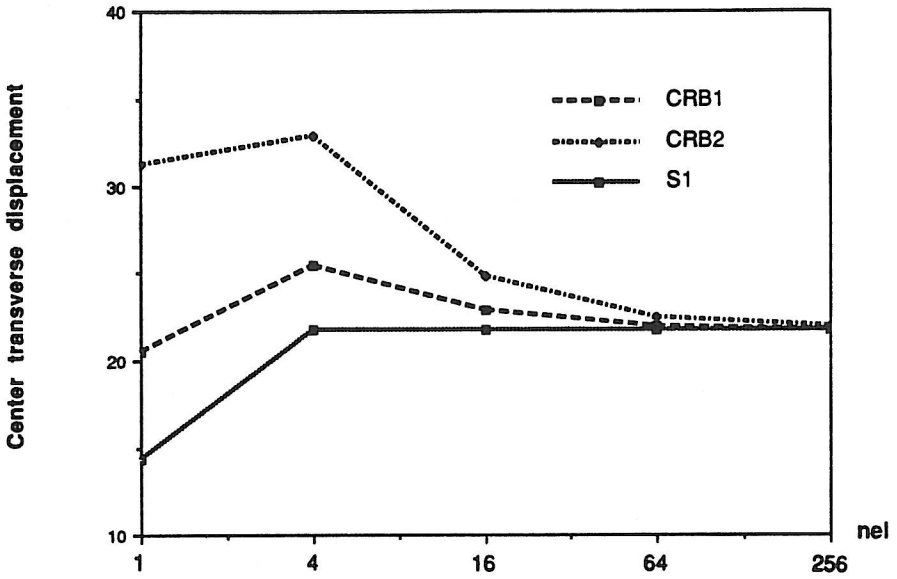

Figure 5.15 - Convergence study for thick square plate; clamped, uniform load.

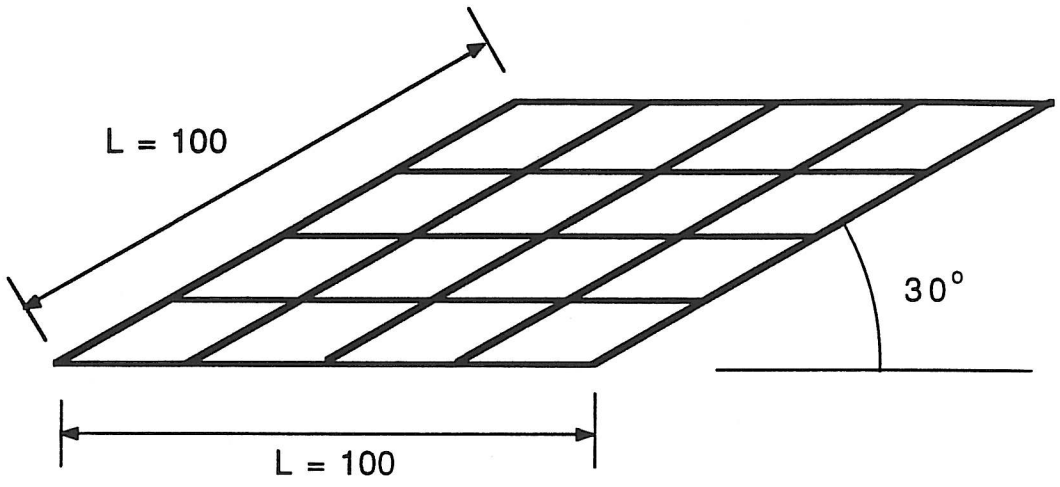

Figure 5.16 - Rhombic plate mesh.

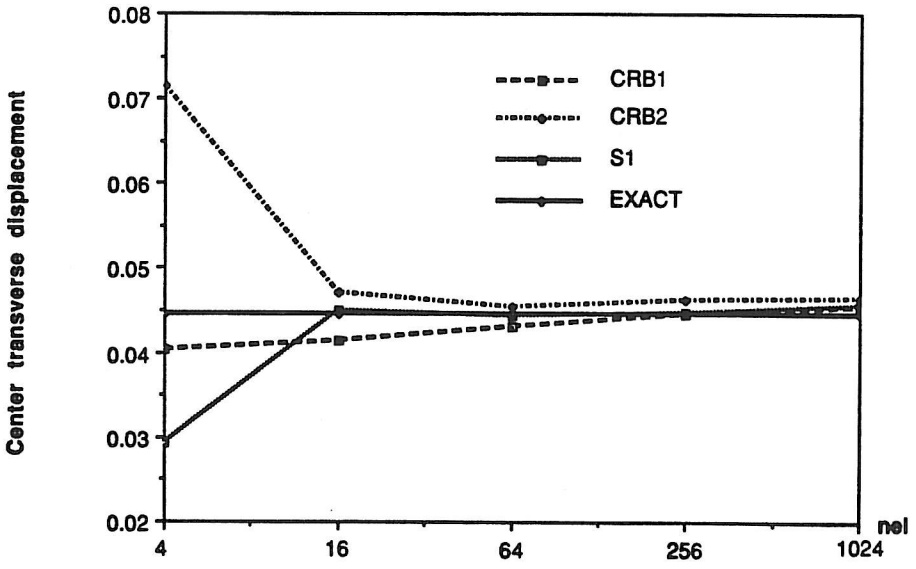

Figure 5.17 - Convergence study for rhombic plate.

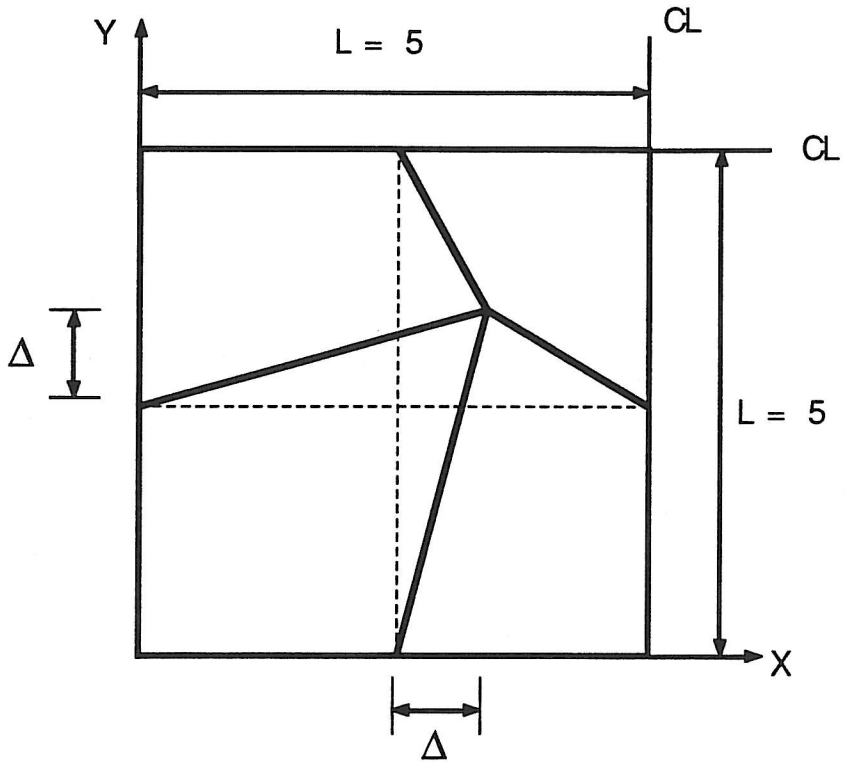

Figure 5.18 - Mesh distortion - symmetric.

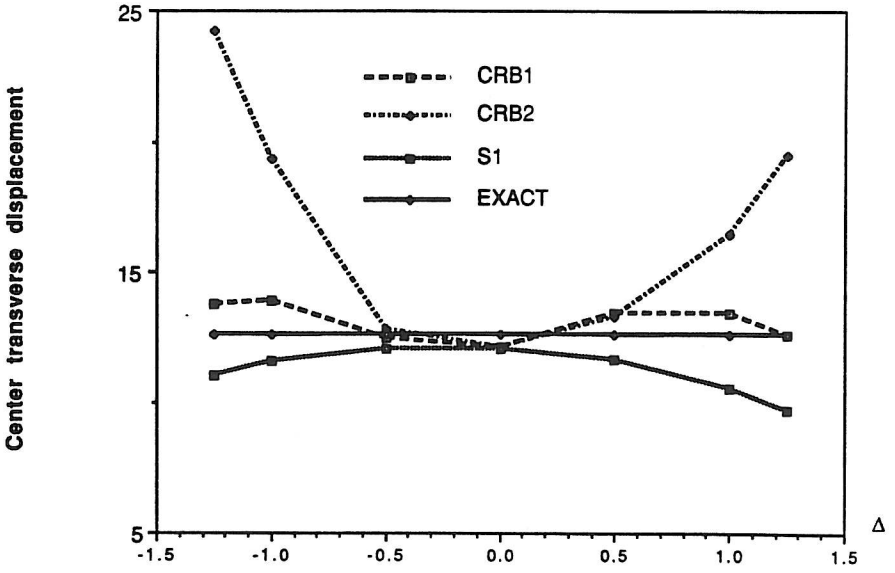

Figure 5.19 - Sensitivity to mesh distortion - symmetric.

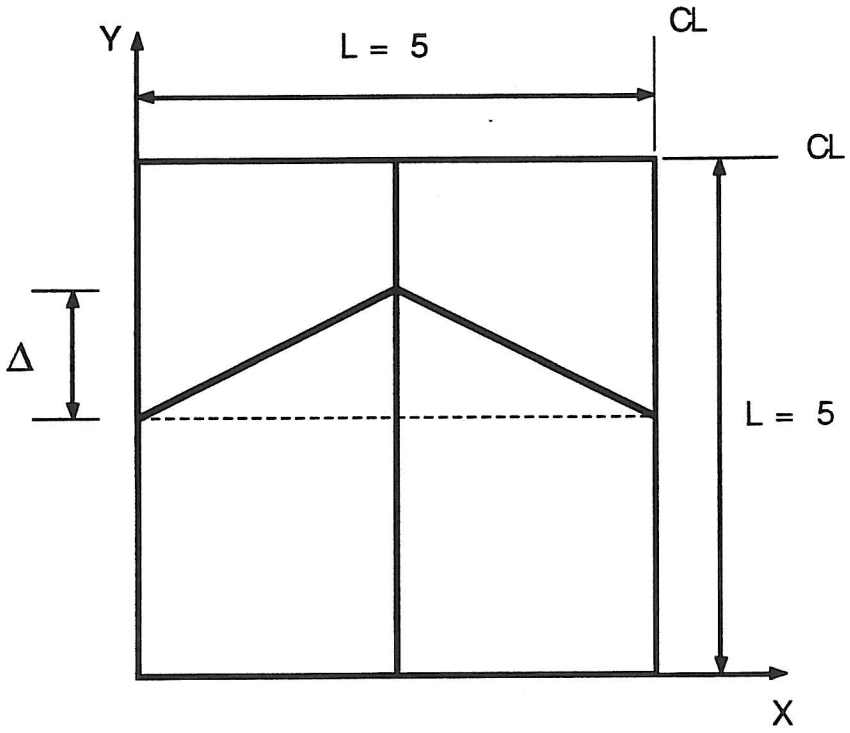

Figure 5.20 - Mesh distortion - asymmetric.

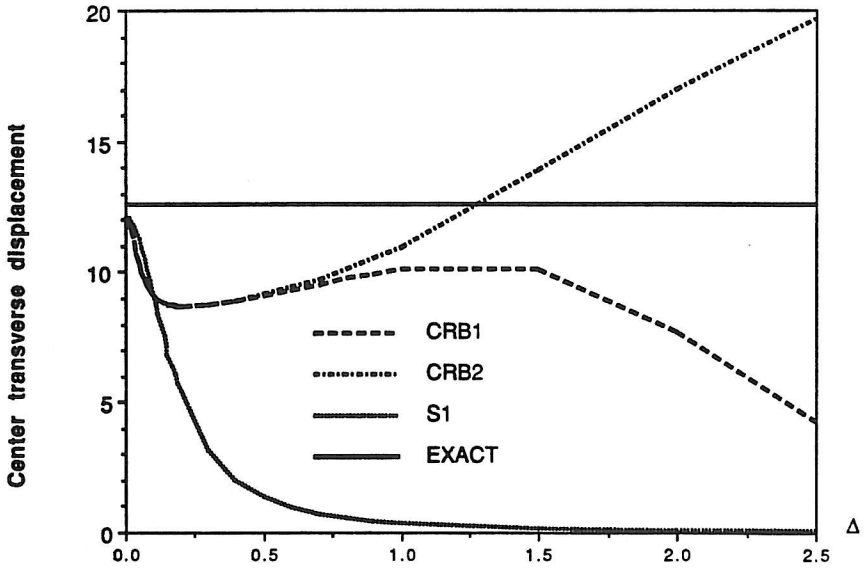

Figure 5.21 - Sensitivity to mesh distortion - asymmetric.